Seasonal variations of Arctic low-level clouds and its linkage to sea ice seasonal variations

Yueyue Yu[1], Patrick C. Taylor[2, *], Ming Cai[3]

[1]*Key Laboratory of Meteorological Disaster, Ministry of Education (KLME)/Joint International Research Laboratory of Climate and Environment Change (ILCEC)/Collaborative Innovation Center on Forecast and Evaluation of Meteorological Disasters (CIC-FEMD), Nanjing University of Information Science and Technology, Nanjing 210044, China*

[2] *NASA Langley Research Center, Climate Science Branch, Hampton, Virginia, USA*

[3]*Department of Earth, Ocean & Atmospheric Sciences, Florida State University, Tallahassee, Florida, 32304, USA*

Correspondence to: Patrick C. Taylor (patrick.c.taylor@nasa.gov)

Key Points:

• Surface type stratification is used to investigate the sea ice coverage influence on the seasonal variation of low-level Arctic clouds

• Sea ice cover has no significant direct influence on the seasonal variation of lower tropospheric cloud liquid water path

• The seasonal variation of lower tropospheric cloud liquid water path is strongly modulated by lower tropospheric stability

Abstract

Using CALIPSO-CloudSat-Clouds and the Earth's Radiant Energy System (CERES)-Moderate Resolution Imaging Spectrometer (MODIS) (C3M) dataset, this study documents the seasonal variation of sea ice, cloud, and related atmospheric properties in the Arctic region (70°N–82°N) during the period 2007–2010. A surface type stratification consisting of four surface types—*Permanent Ocean*, *Land*, *Permanent Ice*, and *Transient Sea Ice*—is used to investigate the surface type influence on low-level Arctic cloud liquid water path (LWP) seasonality. *Transient Ice* regions are further divided into sub-regions according to the melt/freeze season onset dates. Results show no significant dependence of May and September/October low-level cloud LWP peak and melt/freeze onset dates, suggesting that sea ice cover has no significant direct influence on the LWP seasonality. Rather, sea ice cover appears to have an indirect influence by modifying the surface temperature response to increased solar insolation and influencing lower tropospheric stability (LTS). The results suggest that the combined seasonal variations in atmospheric water vapor, due to air temperature changes, and LTS governs the seasonal structure of low-level cloud LWP. Over *Transient Ice* regions, the results suggest that the May peak in LWP coincides with a decrease in LTS and is insensitive to melt and freeze onset. Variations in melt and freeze onset dates are found to influence the cloud LWP probability distribution, where regions of earlier melt and later freeze onset how a higher frequency of larger values.

1. Introduction

One of the factors that make the Arctic region (poleward of 60°N) the most sensitive region to climate change is the large coverage of sea ice and its pronounced seasonal changes (Maslanik et al., 2007; Blunden & Arndt, 2016). By modulating surface albedo, the turbulent heat and momentum fluxes at the ocean–atmosphere interface (Serreze et al., 2007), as well as thermodynamic and radiative processes associated with water vapor, clouds and aerosol feedbacks (see review by Budikova, 2009), Arctic sea ice cover plays an important role in regulating atmosphere-surface energy balance at high latitudes and influencing the large-scale atmospheric circulation (Zhang et al., 2008; Wu & Zhang, 2010; Overland & Wang, 2010; Wu et al., 2014; Taylor et al., 2018). Various indices/parameters have been used to quantify sea ice variability from different perspectives, including the sea ice extent, concentration, thickness, and age (Maslanik et al., 2007; Kwok & Untersteiner, 2011; Stroeve et al., 2012), as well as the melt season timing and length (Perovich et al., 2007; Perovich & Polashenski, 2012; Stroeve et al., 2014; Mortin et al., 2016). The timing of melt onset and its duration are thought to impact the freeze season and subsequent winter ice thickness and volume anomalies (Bitz et al., 1996; Laxon et al., 2003). Among the dynamic and thermodynamic processes responsible for Arctic sea ice variability, cloud-sea ice interactions are one of the most poorly understood aspects and has been the subject of several recent studies (Liu & Key, 2014; Taylor et al., 2015; Letterly et al., 2016; Kay et al., 2016; Morrison et al., 2018). A better understanding of the interaction between sea ice and clouds will provide valuable insights into the Arctic climate system and may ultimately help improve climate simulations.

It is widely accepted that changes in cloud cover and cloud properties play a pivotal role in sea ice growth and melt via changes in Arctic surface radiative and turbulent fluxes (Maykut & Untersteiner, 1971; Shupe & Intrieri, 2004; Shupe, 2011; de Boer et al., 2009; Morrison et

al., 2012; Persson et al., 2002, 2017). Clouds have competing effects, namely causing a reduction of the solar (shortwave, SW) energy flux while simultaneously enhancing the thermal (longwave, LW) radiative energy flux to the surface. The net cloud radiative effect depends on the season and cloud properties, such as cloud phase, cloud optical depth, and cloud base height (Sun & Shine, 1994; Shupe & Intrieri, 2004, Chen et al., 2006). Arctic clouds warm the surface via LW cloud radiative effects most of the year except for a few months in summer when the SW cloud radiative effect dominates (Intrieri et al., 2002; Wang & Key, 2003, 2005; Schweiger & Key, 1994; Morrison et al., 2012; Kay & L'Ecuyer et al., 2013). Low-level clouds, occurring frequently in the Arctic and often comprised of supercooled liquid, have a stronger influence on the surface energy budget than high clouds (e.g., Shupe & Intrieri, 2004; Winton, 2006; Kay & Gettelman, 2009; Kay et al., 2008, 2012). The strong cloud radiative effect makes the low-level liquid clouds an important driver of changes in the surface temperature, growth and melt of sea ice, and regulate the sea ice albedo feedback (Zhang et al., 1996; Kay, 2008; Serreze & Barry, 2011; Wu & Lee, 2012; Liu & Key, 2014; Mortin et al., 2016).

Recent studies point to the important influence of sea ice on Arctic low-level cloud formation, based on results derived from surface observations (Eastman & Warren, 2010; Sato et al., 2012), remotely sensed data (Schweiger et al., 2008; Kay & Gettelman, 2009; Palm et al., 2010; Kay et al., 2011; Liu et al., 2012; Wu & Lee, 2012; Taylor et al., 2015) and observationally-constrained models (Schweiger et al., 2008; Cuzzone & Vavrus, 2011; Vavrus et al., 2011; Kay et al., 2011; Barton &Veron, 2012). Sato et al. (2012) reported that Arctic open water areas tend to have a larger amount of clouds than sea ice covered areas. Model simulations also suggest that low-level clouds occur more frequently and have a larger liquid water path (LWP) during low sea ice cover years (Barton & Veron, 2012). The long-term decreasing trend of sea ice is thus expected to be associated with more low-level clouds (Wu & Lee, 2012) and enhanced Arctic amplification (e.g., Holland & Bitz, 2003; Screen &

Simmonds, 2010; Serreze & Barry, 2011; Vavrus et al., 2009; Yoshimori et al., 2014). The total variance (excluding signals from the annual cycle and linear trend) in cloud cover from July to November may also be explained by the sea-ice–cloud feedback (Liu et al., 2012).

A few studies have attempted to explain how sea ice affects cloud amount. One of the direct atmospheric responses to the Arctic sea ice loss is an increased lower-tropospheric heating and moisture content by surface turbulent fluxes (Francis et al., 2009; Overland & Wang, 2010). The enhanced turbulent heat fluxes from the surface and subsequent horizontal and vertical convergence of moisture and energy can aid in the formation of Arctic clouds (Curry et al., 1995, 1996). Indirectly, a reduction of sea ice cover during boreal fall and winter acts to reduce lower tropospheric static stability and deepen the planetary boundary layer, leading to an enhanced upward moisture transport and favoring cloud formation (Francis et al., 2009; Overland & Wang, 2010; Pavelsky et al., 2011; Taylor et al., 2015; Jun et al., 2016).

Many of the previous Arctic sea ice-cloud interaction studies focused on interannual or longer time scales. It remains an open question to what extent the coupling mechanisms of Arctic sea ice and low-level clouds at interannual scales are relevant at the seasonal scale. This study explores the influence of Arctic sea ice on low-level clouds at seasonal time scales. The seasonal variation of Arctic low-level clouds is determined by many interrelated factors, including the annual cycle of the incoming solar radiation, sea ice coverage, sea ice thickness, and atmospheric meteorological characteristics. In this study, to elucidate the influence of surface type and the seasonal variation of sea ice on the seasonal variation of low-level Arctic clouds, we use the surface type stratification as in Morrison et al. (2018). The surface types include i) *Permanent Ocean* covered by sea ice-free ocean year-round, ii) *Land*, iii) *Permanent Ice* covered by sea ice pack year-round, and iv) *Transient Ice* where there is a significant seasonal change in sea ice coverage, namely covered by sea ice in winter but ice-free ocean in

summer. The *Transient Ice* type regions are further divided into sub-regions according to the onset dates of the melt and freeze seasons.

The remainder of this paper is organized as follows. The data is presented in section 2. Section 3 shows seasonal variations of sea ice coverage as well as their onset dates of melt and freeze seasons; while in Section 4, we present seasonal variations of low-level cloud properties over different surface types. Section 5 examines the key factors that determine seasonal variations of low-level clouds. A summary of our findings is presented in Section 6.

2. Data

The instantaneous cloud property and co-located sea ice concentration (SIC) data for the period from July 2006 through June 2010 is obtained from the Ed RalB1 CALIPSO-CloudSat-Clouds and the Earth's Radiant Energy System (CERES)-Moderate Resolution Imaging Spectrometer (MODIS) (C3M) dataset (Kato et al., 2010). C3M provides column integrated and vertical profiles of cloud properties such as cloud fraction (CF), liquid water content (LWC), and ice water content (IWC) from merged satellite radar-lidar-imager retrievals averaged over CERES footprints, ~20 km. C3M also includes footprint SIC retrievals from the Special Sensor Microwave/Imager (SSM/I) for 2006–2007 and Special Sensor Microwave Imager/Sounder (SSMIS) for 2008 to 2010 (Cavalieri et al., 1996). Cloud liquid and ice water amounts within C3M are derived from a combination of passive retrievals from MODIS radiances using the CERES science team Edition 3 retrieval algorithms (Minnis et al. 2011a; 2011b) and cloud boundary retrievals from CALIPSO and CloudSat. CloudSat-derived ice and liquid water contents are converted to the extinction coefficient using the relationship given by Fu (1996) for ice and by Minnis et al. (1998) for liquid. Note that in Fu (1996), it is assumed that ice crystals are hexagonal. Particle size is required for the conversion from CloudSat radar reflectivity to IWC. If CloudSat particle size is not available, MODIS-derived particle size is

used. The extinction coefficient integrated over all cloud layers in the column is normalized by the optical thickness derived by MODIS (Kato et al., 2011). Ice and liquid phase discrimination is based on CloudSat derived LWC and IWC profiles partitioned using the temperature profile. The cloud water content from CloudSat is 25% smaller than the limited in-situ measurements in the Arctic (Austin et al. 2009). A detailed description of the data can be found in Kato et al. (2010, 2011). The potential biases in these data are not expected to have a strong surface type dependence, meaning that our results relative to different surface types and comparing different regions should be robust even if the absolute values of LWC and IWC are biased.

On any a given day, there are up to 2759 footprints in the latitude band of 70°N–82°N. Because these footprints occur over the same locations about every two weeks, the temporal resolution of the footprint-level data would be very coarse. To increase the temporal resolution, we gridded the footprint-level data—including SIC, vertical profiles of temperature, water vapor, and cloud properties—by averaging all available footprint-level data within a given grid box. When the spatial resolution of the grids is sufficiently coarse, the gridded data would have a daily temporal resolution. The results reported here are obtained at the resolution of 2° in longitude by 0.5° in latitude (about 50km by 50km). This ensures the data at the majority (65%) of grid points has a temporal resolution shorter than 3 days and 95% of grid points have a temporal resolution shorter than a week. We then constructed the 4-year mean (2007–2010) annual cycle at each calendar day from January 1 to December 31 of sea ice concentration (SIC), cloud fraction, water vapor content (WV), cloud liquid water path (LWP), cloud ice water path (IWP), lower tropospheric static stability (LTS), and temperature. This allows us to assess the relationship between the seasonal variations of Arctic clouds and sea ice with respect to the melt and freeze season timing.

The European Centre for Medium-Range Weather Forecasts (ECMWF) Interim Re-Analysis (ERA-Interim) dataset (Dee et al., 2011) show significant improvements in the global hydrological cycle in terms of water vapor, clouds and precipitation in ERA-Interim versus ERA-40, especially over the oceans (Uppala et al., 2008). Considering that, we derive the surface evaporation flux from the ERA-Interim dataset for the period 2007–2010, interpolated to a 2°×0.5° longitude–latitude grid, as the same as the re-gridded C3M data.

3. Seasonal variations of sea ice concentration

We have characterized grid points into 4 types. (i) A grid is called *Land* if the sum of area percentage of ocean and sea ice in that grid is less than 99% over more than 50% of the time[1]; for the grid points not belonging to *Land* type, (ii) *Permanent Ocean* type is a grid where SIC < 15% over 99% of the time; (iii) *Permanent Ice* type is a grid where the SIC exceeds 15% over 99% of the time; (iv) the remaining grids are placed into the *Transient Ice* type. Fig. 1a shows the location of the four surface types indicating that most of the areas within 70°N–82°N are characterized as the *Transient Ice* type. The *Permanent Ocean* surface type lies mainly over the Barents Sea. *Permanent Ice* type is mainly in the Canadian Archipelago region over the longitude bands from 170°W to 90°W at 82°N and the longitudinal coverage shrinks with a decrease in latitude until to a very narrow longitude band around 135°W at 75°N. The northeast of Greenland and Severnaya Zemlya also show several grid points belonging to the *Permanent ice* surface type.

By definition, only sea ice over *Transient Ice* grid points show a pronounced seasonal variation. In this study, we consider spatial patterns of the *onset date of melt season and freeze*

[1] Note that the sum of area percentage of ocean and sea ice (i.e., 100% minus land fraction) for a grid box can vary because of the limited sampling. Each 2°×0.5° grid box is not sampled all of the time and the exact sampling within the grid box differs. Therefore, in this study, we consider the grid box that is not completely covered by ocean or sea ice (i.e., the sum of area percentage of ocean and sea ice in that grid is less than 99%) in more than a half of time as *Land*, which is consistent with the terrain boundary (see Fig. 1a).

183 *season* to characterize the differences in the seasonal variations of Arctic sea ice and their
184 relationship with Arctic low-level clouds. Previous studies used surface temperature,
185 brightness temperature, and sea ice concentration from passive microwave satellite data to
186 detect the first sea ice melt and freeze dates (e.g., Smith, 1998; Kwok et al., 2003; Belchansky
187 et al., 2004; Markus et al., 2009; Stroeve et al., 2014; Collow et al., 2015). Markus et al. (2009)
188 and Stroeve et al. (2014) defined the melt/freeze onset dates based on the sensitivity of
189 microwave brightness temperatures at 19 and 37 GHz to liquid water content in the snow pack.
190 Persson (2012) defined the time when the weekly-mean surface temperature exceeds (falls
191 below) -1.15 °C for the first time as the onset of the melt season (freeze season) and other
192 studies used different melting point around -1.15 °C at different stations and different datasets
193 (Andrew & Ackley, 1982; Lindsay, 1998; Rigor et al., 2000). Collow et al. (2015) determined
194 the melt date as the first day after April 1st at which sea ice concentration drops below 15% and
195 after which the sea ice melt persists until the end of summer (called "continuous melt onset
196 date"). This is in accordance with the traditional definition of sea ice extent from the
197 Intergovernmental Panel on Climate Change assessment report (Vaughan et al., 2013).

198 The C3M data do not provide brightness temperatures at 19 and 37GHz. In addition, a close
199 examination of the time series of surface temperature and SIC at each grid point reveals that
200 the timing of surface temperatures exceeding/below -1.15 °C does not correspond well with
201 the timing of significant increasing/decreasing of SIC at all grid points, which may be related
202 to the local salinity, ice thickness, and other thermodynamic features at specific locations
203 (Fujino et al., 1974; Persson, 2012). Taking these factors into consideration, we define the onset
204 date of melt season at a grid point as the day a) at which its SIC falls below 80% and b) after
205 which its SIC shows a decreasing tendency for more than 80% of the time with the total
206 decrease of SIC exceeding 10% within a one-month period. Condition b) helps to eliminate the
207 situation of sea ice regrowth after any short-lived, random melting events. Similarly, the onset

208 date of the freeze season is defined as the day c) at which SIC increases to 15% observed after
209 the melt season begins, and d) after which its SIC shows an increasing tendency for more than
210 80% of the time with the total increase of SIC exceeding 10% within a one-month period.
211 Again, condition d) helps eliminate the situation of re-melting of SIC after any short-lived,
212 random freeze events. The threshold value of 80% and 15% in condition a) or c) is based on
213 the boundary value of SIC between marginal ice zone and the pack ice (i.e., 80%) and between
214 open ocean and marginal ice zone (i.e., 15%) commonly used by operational ice centers (e.g.,
215 U.S. National Ice Center) and many previous studies (e.g., Parkinson, 2014).

216 According to the probability distribution function (PDF) of the melt and freeze season onset
217 dates in Fig. 2, we can further divide the *Transient Ice* region into four sub-regions where
218 melting starts before May 15, May 16–June 15, June 16–31, and after June, or four sub-regions
219 where freezing starts before October, October 1–15, October 16–31, and after October. In Figs.
220 1b–c, we use different colors to indicate the geographic location of those sub-regions based on
221 melt season onset dates and freeze season onset dates, respectively. In general, Fig. 1 shows
222 that higher latitudes tend to have a later melt season and earlier freeze season, consistent with
223 the seasonal cycle of solar insolation. However, there are large zonal deviations in the timing
224 of the onset of the melt and freeze seasons, indicating that local physical processes (e.g., ice-
225 albedo, water vapor clouds feedbacks) as well as dynamic processes that influence the total
226 energy input at surface also play a major role in the seasonal variations of sea ice. The melt
227 season onset dates range mainly from April to July (Fig. 2). The grid points whose onset date
228 of melt season can be earlier than May 15 (dark blue shadings in Fig. 1b) are located mainly in
229 the rims of the *Permanent Ocean* region and coastal regions adjacent to land. The grid points
230 with a melt onset date after June (yellow shadings in Fig. 1b) are located at higher latitudes and
231 mainly in the longitude band 120°E–150°W. The onset date of the freeze season (Fig. 1c)
232 ranges mainly from September to November (Fig. 2), and the month of October is the starting

month of freezing for most of the grid points. Because the color scheme for Fig. 1c is deliberately set to be in the reverse order as that in Fig. 1b, the spatial pattern of the freeze season onset looks similar to the onset date of melt season, meaning that regions with an earlier melt onset date also tend to have a later freeze onset date or the melt and freeze season onset dates tend to be negatively correlated. It is also seen that the onset date of the melt season is positively correlated with annual mean SIC (Fig. 3) (spatial correlation at about 0.7), while the onset date of the freeze season has a large negative correlation with the annual mean SIC (spatial correlation at about –0.7). This indicates that the late melt season and early freeze season of a region may partially explain the mean value of SIC. Such pronounced correlations among the onset dates of the melt and freeze seasons, and the annual mean SIC have been reported in previous studies (Perovich et al., 2007; Perovich & Polashenski, 2012; Stroeve et al., 2014; Mortin et al., 2016). The results also suggest that the total amount of solar energy absorbed during the summer melt season is more strongly related to the timing of when the melt begins than on the total incident energy. The earlier that sea ice melt begins, the more energy that is stored in the ocean mixed layer, which is then released in the fall for a later freeze season (Kurtz, et al., 2011), potentially delaying the freeze-up and promoting a thinner ice cover for the subsequent year (Dumas et al., 2003; Lindsay & Zhang, 2005). In addition, the sea-ice albedo feedback, which is dominant in summertime, may also help delay freeze onset over regions of smaller sea ice concentration.

We calculated the PDF of SIC over *Transient Ice* grid points for each calendar day from January 1 to December 31. Fig. 4 shows the (4-year) seasonal variations of the PDF of SIC over the grid points that have different onset dates of the melt season (Figs. 4a–d) and freeze season (Figs. 4e–h) as well as considering all *Transient Ice* grid points (Fig. 4i). It is seen that regardless of an early or late melt season onset date, most regions have high values of SIC (above 80%) before onset of melt season and gradually evolve towards a nearly ice-free state

after onset. Most *Transient Ice* grid points reach the ice-free state by September (Figs. 4a–c, about 3–4 months after their onset dates of melting) except for those grid points with a melt onset after-June (Fig. 4d), where the September mean SIC value (black line) is about 40%. The temporal evolution from freeze season onset to an ice-covered state is much faster (about 1–2 months) than that from melt onset to the minimum sea ice state. Such asymmetry in the length between melt and freeze seems to suggest the seasonal variation of duration of daylight is a more dominant factor main factor in determining freeze onset while the role of local and nonlocal feedback processes play a more important role for melt onset.

4. Seasonal variations of low-level cloud liquid water path over different surface types

In this section, we present the seasonal variations of low-level cloud properties below 3 km, which dominates the annual cycle of the total cloud amount as reported by Eastman & Warren (2010). Our analysis focuses on the cloud LWP in the atmospheric layer from the surface to 3 km altitude, which has been reported to have the strongest cloud radiative effects (Shupe & Intrieri, 2004; Winton, 2006; Kay & Gettelman, 2009; Kay et al., 2008, 2012; Mortin et al., 2016) and thus the largest potential impact of surface type and sea ice coverage on cloud LWP and the surface energy budget. A brief discussion on the ice water path (IWP), total water path, as well as cloud fraction is provided below. The cloud LWP is presented as PDFs over the *Transient Ice* regions with different melt and freeze season onset dates as well as over the all *Transient Ice* grids. The latter (without stratifying by onset dates of melt/freeze) can be used as a reference for us to delineate the sensitivity of low-level cloud properties with respect to different onset dates of melt/freeze. We will also show the PDFs of low-level cloud properties over *Land*, *Permanent Ocean*, and *Permanent Ice* as references for us to delineate the sensitivity of low-level cloud properties with respect to different surface types. Because of the large negative correlation between melt and freeze season onset dates, seasonal variations of

cloud properties as well as other atmospheric variables over grid points of *Transient Ice* with different ranges of freeze onset dates can be easily inferred from the seasonal variations over grid points of *Transient Ice* with different ranges of the melt onset dates. For this reason, our discussion if primarily focused on the results obtained by dividing the *Transient Ice* region based on melt onset dates unless the results obtained for different freeze onset dates provide additional information.

Table 1 and the left column of Fig. 5 show that seasonal variations of the low-level cloud LWP exhibits distinct features in terms of both annual mean and temporal evolution over different surface types. Specifically, the annual mean of low-level cloud LWP over *Transient Ice* is 0.21 kg/m^2, smaller than that over *Permanent Ocean* (0.46 kg/m^2) but larger than over *Land* (0.15 kg/m^2) and *Permanent Ice* (0.16 kg/m^2). In cold months (November through April), there is little surface type-dependent difference in low-level cloud LWP over *Land*, *Permanent Ice* and *Transient Ice* surfaces, all showing a small LWP with little spatial variability. Similar findings have been reported in other studies using ground observer and satellite passive radiometer retrieval data (Vowinckel, 1962; Liu et al., 2012). But over *Permanent Ocean*, the low-level cloud LWP is still very high in cold months, with the (areal) mean of above 0.2 kg/m^2 and a noticeable spatial variability. The temporal evolution of the low-level cloud LWP over *Permanent Ocean* shows a continuous increase in the first half year (January-June) and a decrease in the remaining half year. The peak around August has been reported for Arctic Stratus over ocean as well by Klein & Hartmann (1993). Over other surface types, a strong increase in low-level cloud LWP can be seen during warm months (May through September) and a gradual decrease in LWP can be seen after September-October. It is interesting to see that over *Permanent Ice* and *Transient Ice* surfaces, the LWP starts to decrease from mid-May to the end of June, then again increases through mid-August. The local minimum in the seasonal variation of the areal mean LWP around July is less significant over *Transient Ice*

than over *Permanent Ice*, and the spatial variance is quite large in the period from July to September.

We next examine the sensitivity of the PDF of low-level cloud LWP over *Transient Ice* surface with different melt (Figs. 5e-5h) and freeze onset dates (Figs. 5i-5l). The contours in Figs. 5e–5l are differences in the LWP PDF between *Transient Ice* points with different melt season onset dates and all *Transient Ice* grid points, with positive/negative values indicating a larger/smaller percentage of grid points falling into the specific bin of LWP (the ordinate) in comparison with the LWP PDF over all grid points of *Transient Ice* surface shown in Fig. 5b. The results do not show evidence of a shift in the timing of the low-level cloud LWP to earlier/later over earlier/later melting/freezing region and a shift toward later/earlier time over later/earlier melting/freezing regions. This indicates that the onset date of melt/freeze season seems to play a minor role in the seasonal evolution of low-level cloud LWP or the impact of the opening and closing of water surface on the LWP is overwhelmed by other factors. Nevertheless, we can still find some pieces of evidence showing the dependence of cloud LWP on sea ice variation. It is seen from Table 1 and Figs. 5e–5l that the annual mean and range of cloud LWP tend to be larger in earlier/later melting/freezing regions and the reverse can be said for later/earlier melting/freezing regions. The contours in Figure 5, however, indicate that sea ice presence influences probably distribution of cloud LWP. There is a much higher/lower likelihood of larger cloud LWP occurrences in July and August for places that start melting earlier/later. The higher likelihood of larger/smaller cloud LWP values can also be found in places that freeze up later/earlier in October and November, and is larger in the fall than the summer. Furthermore, the earlier/later the melt season begins, the seasonal evolution of low-level cloud LWP is closer to that over *Permanent Ocean*/*Ice* region. The same feature can be found for regions where freeze season begins later/earlier, though less pronounced.

5. Physical processes linking the sea ice to the seasonal variations of low-level LWP over different surface types

According to previous studies (Francis et al., 2009; Overland & Wang, 2010; Pavelsky et al., 2011; Taylor et al., 2015; Jun et al., 2016), sea ice exerts impacts on the Arctic low-level cloud formation mainly by moistening the air and decreasing static stability in the lower troposphere. Therefore, in this section, we will investigate the annual cycle of water vapor content below 3 km and the lower tropospheric static stability (LTS) over different surface types to address the following questions: Why is the annual mean and annual cycle of the low-level cloud LWP dependent on the surface type, while the timing LWP annual cycle over *Transient Ice* surface shows a weak dependence on the regional difference in the melt season onset dates? What factors (besides sea ice variation) play a dominant role in the seasonal variation of LWP? Are these factors modified by the nature of underlying surface?

5.1 Moisture condition

Seen from Table 1, the annual mean of water vapor in the lower troposphere below 3 km shifts from larger to smaller values when the surface type changes in the order of *Permanent Ocean*, *Transient Ice*, *Permanent Ice*, and *Land*. Among the *Transient Ice* regions with different ranges of melt season onset dates, the annual mean value of water vapor tends to be larger over earlier melting regions. This is consistent with the dependence of annual mean LWP on the surface type, which supports an important role of lower tropospheric water vapor in maintaining dense low-level clouds explaining the sensitivity of annual mean cloud LWP to surface type and SIC. Such dependence of the annual mean water vapor on the underlying surface type could result from the local evaporation rate tied to the surface type and SIC; the annual mean, regionally-averaged surface evaporation rate from ERA-Interim shows similar dependence on the surface type (Table 1). But it is noteworthy to point out that factors other

than evaporation affect the regional difference in the annual mean water vapor in the lower troposphere such as air temperature, atmospheric advection from lower latitudes, and surface temperature dependent on the latitude or solar zenith angle.

The seasonal variation of water vapor below 3 km shown in Fig. 6 indicates small water vapor amounts in the atmosphere during cold months over the frozen surface (including *Land*, *Permanent Ice*, and *Transient Ice* surfaces), whereas the air above *Permanent Ocean* contains a larger amount of moisture (about 3 cm). *Permanent Ocean* exhibits the strongest evaporation rate in winter, whereas the other surface types have an evaporation rate close-to-zero (Figs. 7a–d). In warm months, despite that the strongest increase in atmospheric water vapor from cold months over the *Permanent Ocean* and *Transient Ice* surfaces, atmospheric moisture becomes abundant everywhere and the temporal evolution of lower tropospheric water vapor over all surface types increases beginning in April, reaching a single peak value around the end of July and the beginning of August and decreasing afterwards. Such a temporal evolution in warm months follows the air temperature and the annual cycle of sunlight rather than the seasonality of surface evaporation rate. Similar results are found in the seasonal variations of atmospheric moisture and surface evaporation rate in *Transient Ice* regions with different melt season onset dates (Figs. 6e–h and Figs. 7e–h). In particular, in regions where the melt season begins earlier/later (where SIC tends to be smaller), the evaporation tends to be stronger especially in cold months and the second increase in late summer due to the entirely opening of the water surface tends to occur earlier and stronger. However, comparing Figs. 7e–h with the areal mean temporal change of water vapor shown in Figs. 6e–h, the contribution from local evaporation to the water vapor change appears small. This confirms the findings reported by Solomon et al. (2011) that water vapor from the surface layer is not efficiently transported into the cloud layer because the surface layer below the lower entrainment zone is frequently decoupled from the cloud mixed-layer system.

The temporal variation of lower tropospheric moisture is not consistent with that of low-level cloud LWP over *Permanent Ice* and *Transient Ice* regions in warm months, indicating that the seasonal variations of the total moisture in the lower troposphere does not completely explain the seasonal variation of LWP. Over *Permanent Ocean*, cloud LWP more closely follows the water vapor annual cycle. This is because the cloud forming mechanisms are more active in the *Permanent Ocean* region, which is primarily the north Atlantic Ocean and characterized by frequent large-scale uplift from extratropical cycles and warm advection. Those unique atmospheric conditions more efficiently convert water vapor into LWP. Therefore, the role of total moisture in the lower troposphere appears to not dominate the seasonal evolution of the low-level cloud LWP in warm months.

5.2 Atmospheric thermodynamic properties

Seasonal variations in atmospheric thermodynamic properties such as lower tropospheric stability (LTS) also affect cloud formation. In this section, we investigate the seasonal variation of LTS, in conjunction with seasonal variations of surface skin temperature (T_s) and air temperature at 700 hPa (T_{700hPa}), over different surface types. LTS is defined as the difference between the potential temperature at 700 hPa and the surface (e.g., Slingo, 1987; Klein & Hartmann, 1993; Klein, 1997).

The results indicate that seasonal variations in LTS over *Permanent Ocean* exhibits a maximum of about 20 K in summer and a minimum in winter (Fig. 8a), whereas *Land* surfaces show the opposite variation with a maximum LTS >30 K in winter and a minimum in summer (Fig. 8d). This is consistent with previous studies on the LTS in mid-latitude land and ocean regions and can be explained by the different heat capacity of ocean water and land surface as well as latent heat flux at the boundary of ocean and atmosphere (Frierson & Davis, 2011; Pavelsky et al. 2011). The seasonal variation of LTS over *Permanent Ice* (Fig. 8c) is similar to

that over *Land*, other than a small increase in June and July. Over *Transient Ice*, the seasonal variation of LTS (Fig. 8b) resembles *Land* and *Permanent Ice* in cold months (October-April, or during the freeze season) and resembles *Permanent Ocean* in warm months (May-September, or during the melt season). These LTS seasonal variations agree well with the annual cycle of LTS over the Beaufort-Chukchi Seas seasonal ice zone reported by Liu & Schweiger (2017).

To assess which temperature, surface or atmospheric, controls the characteristics of the seasonal variation of LTS over different surface types, we examine the seasonal evolution of T_s (Fig. 9) and T_{700hPa} (Fig. 10). It is expected that the contrast in T_{700hPa} among different surface types is relatively weak because its spatial pattern is mainly determined by atmospheric large-scale advection. The surface temperature, however, exhibits a strong dependence on surface type (Fig. 9). The large contrast in thermal inertia between *Permanent Ocean* and *Land* indicates that their seasonal variations would be different. Because of melting and freezing in the ice-covered regions, particularly in *Transient Ice* regions, the seasonal variation would be similar to *Land* and *Permanent Ice* in cold months and to *Permanent Ocean* in warm months. The processes of melting and freezing would also impact transitions over *Transient Ice* from winter to summer (during melt season) and from fall to winter (during freeze season), making them distinctly different from *Land* or *Permanent Ocean*. In light of the aforementioned discussions, we expect the seasonal variations of LTS over different surface types to be influenced mainly by the thermodynamic properties of the surface.

In cold months, the large thermal inertia and oceanic heat storage keeps the *Permanent Ocean* surface above-freezing (Fig. 9a), while the temperature over the other three surfaces is -10 to -40°C (Figs. 9b–9d). Therefore, the leading factor causing the minimum LTS in cold months over *Permanent Ocean* is the large thermal inertia of the ocean, while the smaller

thermal inertia of the frozen part of Arctic Ocean and ice/snow covered land is responsible for the maximum LTS in cold months. From spring to midsummer, sea surface temperature warming is weaker than the air, due to large heat capacity of ocean explain the increase in LTS over *Permanent Ocean* from the spring to midsummer, responsible for the peak of LTS in summer months (Fig. 8a). Frozen (including *Transient Ice* and *Permanent Ice*) and *Land* surfaces warms more rapidly than the air at 700 hPa in spring, causing a rapid decrease of LTS in early spring (Figs. 8b–8d). Because of the smaller thermal inertia, *Land* surface warming contributes from the spring to midsummer whereas air warming is less significant. As a result, the LTS over *Land* reaches its minimum in summer (Fig. 8d). Over ice-covered regions, because part of the incoming solar energy is used to melt ice instead of warming the surface when the ocean is still covered by a large fraction of ice and because the large heat capacity of ocean after ice melts, surface warming from spring to midsummer over the *Transient Ice* region (Figs. 9b and 9c) is slower than that in the air (Figs. 10b and 10c). These factors explain the summer peak of LTS over *Transient Ice* surface. From the late summer to early autumn, the LTS decreases again because the air at 700 hPa as cools in response to the decrease of sunlight. The above is also applicable to the *Permanent Ice* surface although its seasonal variation has a weaker amplitude in comparison to *Transient Ice* region.

Among the *Transient Ice* surface type, regions with different melt onset dates show generally consistent seasonal variations in LTS (Figs. 8e–8h), as do seasonal variations of T_s (Figs. 9e–9h) and T_{700hPa} (Figs. 10e–10h). However, there are noticeable differences. First, the earlier melting regions show a larger spread in LTS in wintertime, with some grid points following the LTS annual cycle over *Permanent Ocean* and the remaining following *Permanent Ice* in accordance with the differences in annual mean SIC. Second, the earlier melting regions, where there tends to be less SIC, have smaller values of LTS year-round compared with the remaining regions, and the opposite can be said for later melting regions.

453 This confirms the negative correlation found between LTS and SIC reported by Pavelsky et al.
454 (2011). Third, we can see a slight time shift of the end of the decrease of LTS in the early spring
455 and the beginning of the decrease of LTS in the late summer between the earliest melting region
456 (where melt season starts before May 15) and the latest melting region (where melting starts
457 after June). Specifically, over the earliest melting region, the decrease of LTS in the early spring
458 tends to be terminated earlier (Fig. 8e) because the surface temperature is higher in wintertime
459 reaches the melting point as early as the late-April maintaining this temperature for a period of
460 several weeks (Fig. 9e), while the air temperature at 700 hPa (Fig. 10e) catches up. The opposite
461 can be said for the latest melting region (panel (h) of Figs. 8–10). Also, the timing of the rapid
462 decrease of LTS in the late summer tends to start earlier/later over the earliest/latest melting
463 regions. By June or early July, most ice over the earliest melting regions is already melted (Fig.
464 4e) and therefore more energy is available to warm the water surface, causing the skin
465 temperature to increase (Fig. 9e), contributing to the LTS decrease after mid-July (Fig. 8e). In
466 contrast, in regions with the latest melt onset, the surface would not become open water
467 completely until August and September, if at all (Fig. 4h). As a result, the timing of the above-
468 freezing surface temperature increase (Fig. 9h) and decrease in LTS (Fig. 8h) is delayed until
469 August.

470 Next, we investigate the spatial pattern of the relationship between low-level cloud LWP,
471 LTS and lower tropospheric water vapor in warm months (Fig. 11). This helps illustrate how
472 individual surface types may influence the low-level cloud LWP via modifying water vapor
473 and LTS. As expected from Fig. 5 and Fig. 8, the LWP and water vapor below 3 km are
474 positively correlated over the entire Arctic from April to October when the low-level cloud
475 LWP shows the largest seasonality (Fig. 11a), confirming that the increase of atmospheric
476 moisture in summertime favors the formation of clouds with more LWP. On the other hand,
477 the negative correlation between the seasonal variation of LTS and LWP over *Permanent Ice*

and most of the *Transient Ice* regions (Fig. 11b) is consistent with correspondence between the an increased LTS and a decreased low-level cloud LWP during months from April to October (cf. Figs. 5c–d and Figs. 8c–d). The maximum values of negative correlation are found in the *Permanent Ice* region and the negative correlation tends to be smaller over earlier melting regions and part of Greenland. Over the *Permanent Ocean* region, where there is abundant water vapor year-round (Fig. 7a), the correlation between LTS and LWP is positive. This is because low-cloud layers tend to be coupled to the surface over the *Permanent ocean* region, thus a stronger inversion acts to trap more moisture within over marine boundary, permitting greater low-level cloud cover rather than upper-level clouds (Klein & Hartmann, 1993; Wood & Hartmann, 2006; Wood & Bretherton, 2006; Zhang et al., 2009). Another contribution to the positive correlation between LTS and LWP over *Permanent Ocean* is that the clouds in these regions are more strongly influenced by extratropical cyclones. Contrarily, clouds in the *Transient Ice* regions tend to be decoupled from the surface during the warm season (Shupe et al., 2013), are less influenced by extratropical cyclones, and take on the form of persistent stratus or stratocumulus. Thus, the LTS and LWP over *Transient Ice* is overall negatively correlated. However, the negative correlation between LTS and LWP becomes weaker after July when most of the sea ice has melted and can be seen less clearly over earlier melting regions where there is more water vapor than in the later melting regions (cf. Figs. 5e–5h and Figs. 8e–8h, Fig. 11b), contributing to the slightly larger variation of LWP in July and August over earlier melting regions (Fig. 5e).

We also note that the inverse relationship between LWP and LTS is found in terms of the annual mean and variability. Specifically, over the earlier melting region where LTS tends to have a smaller annual mean and larger spread, the LWP also shows smaller annual mean and larger spread, and vice versa (cf. Figs. 5e–h and Figs. 8e–h). Consistent with previous studies (Solomon et al., 2011; Barton et al., 2012), these results suggest that except in cold months

503 when there is a lack of water vapor supply from the frozen surface and air temperature is low,
504 LTS plays a more important role in controlling the cloud properties. The influence of LTS on
505 low-cloud properties is because these clouds often have a moisture inversion near cloud top
506 (e.g., Morrison et al., 2012; Shupe et al. 2013; Solomon et al., 2014). Thus, a weaker cloud-top
507 inversion (weaker LTS) allows more moist air from above the cloud to be entrained into the
508 cloud, thus increasing the cloud LWP. In wintertime, the LWP over surfaces except *Permanent*
509 *Ocean* stays is small due to lack of water vapor and low air temperature, and strong LTS (cf.
510 Fig. 5 and Fig. 8).

511 Another point to be made here is that the cloud microphysics and specifically the cloud
512 phase change due to warming air temperatures appears to not play a role in the differences in
513 cloud LWP by surface type, because as we can see from the Fig. 10, the 700 hPa temperature
514 is similar across the different surface types. In addition, the warmest air temperatures are found
515 around July and do not align with the largest LWP values (Fig. 5), which if cloud microphysics
516 were a dominating influence would be expected to correspond to the timing of the largest LWP.
517 Thus, we argue that microphysics is not the primary factor controlling the seasonal variation
518 of low-level cloud LWP in the Arctic.

519 ***5.3 Seasonal variation of other cloud properties and their dependence on surface types***

520 So far, we reported mainly that the possible impact of sea ice variation on the seasonal
521 variation of cloud liquid water path. Besides that, we also investigated the seasonal variations
522 of the IWP of low-level clouds (Fig. 10), which appear to mainly follow air temperature and
523 are less dependent on the surface type, namely that the IWP always has larger values in cold
524 months and is close-to-zero values in warm months for all surface types. It is further seen from
525 Figs. 10e–h and Table 1 that earlier/later melting regions tend to have less/more annual mean
526 IWP than the remaining *Transient Ice* region, which may be partly attributed to the air

temperature difference among these regions in winter. The only noticeable difference in the temporal evolution of IWP among the four different surface types is found over *Permanent Ocean* where the seasonal variation of IWP from winter to spring is stronger than other surface types. The low-level total water path as well as the cloud fraction is dominated by LWP in warm months and IWP in cold months, thus showing the strongest dependence on surface type in warm months as well (not shown).

6. Summary and Conclusion

This study uses C3M data, a merged data product out of the NASA A-Train satellite constellation, to document the seasonal variation of sea ice, clouds, and the related atmospheric properties in the Arctic region (70°N–82°N) for the period 2007–2010. In so doing, we have converted the footprint-level, C3M data to gridded data set by averaging all available footprint-level data at any a given day within each grid. The results reported here are obtained at the resolution of 2-degree in longitude by 0.5-degree in latitude (or about 50km by 50km), which ensures the data at 65% of grid points would have a temporal resolution shorter than 3 days and 95% of grid points have a temporal resolution shorter than a week.

We use a surface type stratification to investigate the influence of surface type on the seasonality of Arctic low cloud liquid water path. Four surface types are defined: i) *Permanent Ocean* where is open water all the year round, ii) *Land*, iii) *Permanent Ice* where is covered by sea ice pack all the year round, and iv) *Transient Ice* where there is a significant seasonal change in sea ice coverage, namely covered by sea ice in winter but open water in summer. The *Transient Ice* type regions are further divided into four sub-regions according to the onset dates of melt/freeze season based on the SIC daily tendency. Over regions with earlier/later melt season onset dates, the freeze season tends to occur later/earlier. Therefore, results derived

over grid points of transient ice with different freeze onset can be largely inferred from seasonal variation with different melt onset. Key findings in this study are as follows:

i) The annual mean low-level cloud LWP shows a strong dependence on the surface type as listed in Table 1. The open water surface stores solar energy in warm months and releases this energy to air near surface in cold months. Regions with less open water coverage or larger sea ice coverage tend to have a higher temperature in warm months near surface, stronger evaporation, more moisture, and weaker LTS, which describe condition favorable for low-level cloud formation and larger LWP. However, the regional differences in the annual mean cloud LWP are also affected by other factors, such as air temperature, atmospheric advection, lower tropospheric stability, surface temperature.

ii) The seasonal variation of LWP shows a large contrast among different surface types from Spring to Fall, whereas in cold months, due to the lack of water vapor and cold temperatures, the LWP is close to zero over all surface types except *Permanent Ocean*. From Spring to Fall, the decrease in LTS generally corresponds to an increased LWP over surfaces except *Permanent Ocean*, suggesting the important role of atmospheric static instability in the upward mixing of water vapor from near surface and/or access to free tropospheric moisture advected from lower latitudes. Over *Permanent Ocean,* where there is abundant water vapor, smaller LTS, and the influence of extratropical cyclones, the increasing/decreasing of LTS corresponds to an increase/decrease in the low-level cloud LWP. The temporal evolution of water vapor, however, shows little contrast among surface types since it simply follows the annual cycle of temperature and sunlight rather than the evaporation flux annual cycle. Thus, the surface evaporation flux makes a small contribution to the different temporal evolution of LWP dependent on surface types.

iii) The seasonal variation of LTS are influenced mainly by the thermodynamic contrast among different surface types. The melting and freezing in the transient ice regions make the

seasonal variations of surface temperature similar to land in cold months and similar to ocean in warm months. The large contrast in the thermal inertia between ocean, sea ice, and land leads to differences in the seasonal variations of surface temperature, especially for the transient ice regions in the transitions between winter to summer (during melt season) and from fall to winter (during freeze season), while the contrast in T_{700hPa} among different surface types is much weaker.

iv) Among the *Transient Ice* regions, the seasonal variation of low-level cloud LWP over later melting regions is more like that over *Permanent Ice* region, while the LWP over earlier melting regions shows larger values and spread in July and August, closer to that over *Permanent Ocean*. The same feature can be found for regions where freeze season begins later/earlier, though less pronounced. The higher/lower likelihood of larger cloud LWP occurrences for areas that start melting earlier/later is found most significant in melt season, while the higher likelihood of larger/smaller cloud LWP values for places that start freezing later/earlier is found most significant in Fall. This suggests that the variability of low-cloud LWP exhibits a dependence on sea ice variability. Nevertheless, we do not see a clear shift in average seasonal cycle of low-cloud LWP toward earlier/later time over earlier/later melting regions. This lack of sensitivity to the melt onset date suggests that the annual variation in sea ice is not a primary factor controlling the timing of key turning points of the annual cycle of low-level cloud LWP. Our results show that the primary control on the annual cycle of low-level cloud LWP is the ample water vapor in the lower troposphere during the warm season and the inverse relation between LTS and LWP over *Land and Transient ice*.

In closing, our results argue that the primary factor controlling the seasonality of low-level cloud LWP over *Transient ice* regions is the lower tropospheric stability. Thus, the seasonality of Arctic sea ice does not appear to play a significant role in controlling the annual cycle of Arctic low clouds. This refined understanding serves as a useful constraint to assess and

improve the representation of the Arctic cloud annual cycle in climate models and improve the fidelity of Arctic climate change projections.

Acknowledgments and data

This work was supported by grants from the National Science Foundation of China (41705039), the Priority Academic Program Development of Jiangsu Higher Education Institutions (PAPD), and the NASA Interdisciplinary Studies Program grant NNH12ZDA001N-IDS. The processing of the C3M data used in this analysis was funded under the NASA Energy and Water Cycle Studies program and is available from the Langley Atmospheric Science Data Center (http://eosweb.larc.nasa.gov).

Reference:

Andreas, E. L., & Ackley, S. (1982). On the differences in ablation seasons of Arctic and Antarctic sea ice. Journal of Atmospheric Sciences, 39, 440–447.

Austin, R. T., Heymsfield, A. J., & Stephens, G. L. (2009). Retrieval of ice cloud microphysical parameters using the CloudSat millimeter-wave radar and temperature. Journal of Geophysical Research: Atmosphere, 114, D00A2

Barton, N. P., S. A. Klein, J. S. Boyle, and Y. Y. Zhang (2012), Arctic synoptic regimes: Comparing domain-wide Arctic cloud observations with CAM4 and CAM5 during similar dynamics. Journal of Geophysical Research: Atmospheres (1984–2012), 117(D15).

Barton, N. P., & Veron, D. E. (2012). Response of clouds and surface energy fluxes to changes in sea-ice cover over the Laptev Sea (Arctic Ocean), Climate Research, 54, 69–84. https://doi.org/10.3354/cr01101

Belchansky, G. I., Douglas, D. C., & Platonov, N. G. (2004). Duration of the Arctic sea ice melt season: regional and interannual variability, 1979–2001. Journal of Climate, 17, 67–80.

Bitz, C. M., Battisti, D. S., Moritz, R. E., & Beesley, J. A. (1996). Low-frequency variability in the Arctic atmosphere, sea ice, and upper-ocean climate system. Journal of Climate, 9, 394–408.

Blunden, J., & Arndt, D. S. (2016). State of the Climate in 2015, Bull. American Meteorological Society, 97, Si–S275. https://doi.org/10.1175/2016BAMSStateoftheClimate.1

631 Budikova, D. (2009). Role of Arctic sea ice in global atmospheric circulation: A review. Global
632 Planetary Change, 68, 149–163.

633 Cavalieri, D. J., Parkinson, C. L., Gloersen, P., & Zwally, H. J. (1996). Sea ice concentrations
634 from nimbus-7 SMMR and DMSP SSM/ISSMIS passive microwave data, version 1.
635 NASA National snow and ice data center distributed active archive center. Digital data,
636 Boulder, Colorado USA. https ://doi.org/10.5067/8GQ8LZQVL0 VL

637 Chen, Y. H., Aires, F., Francis, J. A., & Miller, J. R. (2006). Observed relationships between
638 arctic longwave cloud forcing and cloud parameters using a neural network, Journal of
639 Climate, 19, 4087–4104. https://doi.org/10.1175/JCLI3839.1

640 Chen, Y. H., Miller, J. R., Francis, J. A., & Russell, G. L. (2011). Projected regime shift in
641 Arctic cloud and water vapor feedbacks, Environmentl Research Letter, 6, 044007.
642 https://doi.org/10.1088/1748-9326/6/4/044007

643 Collow, T. W., Wang, W., & Kumar, A. (2015). Prediction of Arctic Sea Ice Melt Date as an
644 Alternative Parameter for Local Sea Ice Forecasting, Science and Technology Infusion
645 Climate Bulletin, 40th NOAA Annual Climate Diagnostics and Prediction Workshop,
646 Denver, CO, USA, 26–29 October 2015, 26–29.

647 Curry, J. A., Schramm, J. L., Serreze, M. C., & Ebert, E. E. (1995). Water vapor feedback over
648 the Arctic ocean, Journal of Geophysical Research, 100, 14223–14229.

649 Curry, J. A., Rossow, W. B., Randall, D., & Schramm, J. L. (1996). Overview of Arctic cloud
650 and radiation characteristics, Journal of Geophysical Research, 9, 1731–1764.

651 Cuzzone, J., & Vavrus, S. (2011). The relationships between Arctic sea ice and cloud-related
652 variables in the ERA-Interim reanalysis and CCSM3, Environmental Research Letter,
653 6, 014016. https://doi.org/10.1088/1748-9326/6/1/014016

de Boer, G., Eloranta, E., & Shupe, M. (2009). Arctic mixed-phase stratiform cloud properties from multiple years of surface-based measurements at two high-latitude locations, Journal of Atmospheric Sciences, 66, 2874–2887.

Dee, D. P., et al. (2011). The ERA-Interim reanalysis: configuration and performance of the data assimilation system. Quarterly Journal of Royal Meteorological Society, 137, 553–597.

Doyle, J. G., Lesins, G., Thackray, C. P., Perro, C., Nott, G. J., Duck, T. J., Damoah, R., & Drummond, J. R. (2011). Water vapor intrusions into the high Arctic during winter. Geophysical Research Letter, 38, L12806. https://doi.org/10.1029/2011GL047493

Dumas, J. A., Flato, G. M., & Weaver, A. J. (2003). The impact of varying atmospheric forcing on the thickness of arctic multi-year sea ice, Geophysical Research Letter, 30(18), 1918. https://doi.org/10.1029/2003GL017433

Eastman, R., & Warren, S. G. (2010). Interannual variations of Arctic cloud types in relation to sea ice, Journal of Climate, 23, 4216–4232. https://doi.org/10.1175/2010JCLI3492.1

Francis, J. A., Chan, W., Leathers, D. J., Miller, J. R., & Veron, D. E. (2009). Winter Northern Hemisphere weather patterns remember summer Arctic sea-ice extent. Geophysical Research Letter, 36, L07503.

Frierson, D. M. W., & Davis, N. A. (2011). The seasonal cycle of midlatitude static stability over land and ocean in global reanalyses. Geophysical Research Letter, 38, L13803. https://doi.org/10.1029/2011GL047747

Fu, Q. (1996). An accurate parameterization of the solar radiation properties of cirrus clouds for climate models, Journal of Climate, 9, 2058–2082.

Fujino, K., Lewis, E. L., & Perkin, R. G. (1974). The freezing point of seawater at pressures up to 100 bars, Journal of Geophysical Research, 79, 1792–1797.

678 Holland, M. M., & Bitz, C. M. (2003). Polar amplification of climate change in coupled models,
679 Climate Dynamics, 21, 221–232.

680 Intrieri, J. M., Fairall, C. W., Shupe, M. D., Persson, P. O. G., Andreas, E. L., Guest, P. S., &
681 Moritz, R. E. (2002). An annual cycle of Arctic surface cloud forcing at SHEBA,
682 Journal of Geophysical Research, 107, 8039. https://doi.org/10.1029/2000JC000439

683 Jun, S. Y., Ho, C.-H., Jeong J.-H., Choi, Y.-S., and Kim B.-M. (2016). Recent changes in winter
684 Arctic clouds and their relationships with sea ice and atmospheric conditions. Tellus
685 Series A, 68, 29130. https://doi.org/10.3402/tellusa.v68.29130

686 Kato, S., Sun-Mack, S., Miller, W. F., Rose, F. G., Chen, Y., Minnis, P., & Wielicki, B. A.
687 (2010), Relationships among cloud occurrence frequency, overlap, and effective
688 thickness derived from CALIPSO and CloudSat merged cloud vertical profiles. Journal
689 of Geophysical Research Atmosphere, 115(D4).

690 Kato, S., et al. (2011). Improvements of top-of-atmosphere and surface irradiance
691 computations with CALIPSO-, CloudSat-, and MODIS-derived cloud and aerosol
692 properties, Journal of Geophysical Research, 116, D19209.
693 https://doi.org/10.1029/2011JD016050

694 Kay, J. E., L'Ecuyer, T., Gettelman, A., Stephens, G., & O'Dell, C. (2008). The contribution
695 of cloud and radiation anomalies to the 2007 Arctic sea ice extent minimum,
696 Geophysical Research Letter, 35, L08503. https://doi.org/10.1029/2008GL033451

697 Kay, J. E., Hillman, B. R., Klein, S. A., Zhang, Y., Medeiros, B., Pincus, R., Gettelman, A.,
698 Eaton, B., Boyle, J., Marchand, R., & Ackerman, T. P. (2012), Exposing global cloud
699 biases in the Community Atmosphere Model (CAM) using satellite observations and
700 their corresponding instrument simulators. Journal of Climate, 25, 5190–5207.

Kay, J. E., & L'Ecuyer, T. (2013). Observational constraints on Arctic Ocean clouds and radiative fluxes during the early 21st century, Journal of Geophysical Research: Atmosphere, 118, 7219–7236.

Kay, J. E., L'Ecuyer, T., Chepfer, H., Loeb, N., Morrison, A., & Cesana, G. (2016). Recent advances in arctic cloud and climate research, Current Climate Change Reports, 2, 159. https://doi.org/10.1007/s40641-016-0051-9

Kay, J. E., Holland, M. M., & Jahn, A. (2011). Inter-annual to multi-decadal Arctic sea ice extent trends in a warming world, Geophysical Research Letter, 38, L15708. https://doi.org/10.1029/2011GL048008

Kay, J. E., & Gettelman, A. (2009). Cloud influence on and response to seasonal Arctic sea ice loss, Journal of Geophysical Research, 114, D18204. https://doi.org/10.1029/2009JD011773

Klein, S. A., & Hartmann, D. L. (1993). The seasonal cycle of low stratiform clouds, Journal of Climate, 6, 1587–1606.

Klein, S. A. (1997). Synoptic variability of low-cloud properties and meteorological parameters in the subtropical trade wind boundary layer. Journal of Climate, 10, 2018–2039.

Kurtz, N. T., Markus, T., Farrell, S. L., Worthen, D. L., & Boisvert, L. N. (2011). Observations of recent Arctic sea ice volume loss and its impact on ocean–atmosphere energy exchange and ice production. Journal of Geophysical Research, 116, C04015. http://dx.doi.org/10.1029/2010JC006235

Kwok, R., Cunningham, G., & Nghiem, S. (2003). A study of the onset of melt over the Arctic Ocean in RADARSAT synthetic aperture radar data. Journal of Geophysical Research, 108(C11), 3363. http://dx.doi.org/10.1029/2002JC001363

Kwok R., & Untersteiner, N. (2011). The thinning of Arctic sea ice, Physics Today, 64, 36-41.

725 Laxon, S., Peacock, N., & Smith, D. (2003). High interannual variability in sea ice thickness
726 in the Arctic region. Nature, 425, 947–950.

727 Letterly, A., Key, J., & Liu, Y. (2016). The influence of winter cloud on summer sea ice in the
728 Arctic, 1983–2013. Journal of Geophysical Research: Atmosphere, 121, 2178–2187.
729 https://doi.org/10.1002/2015JD024316

730 Lindsay, R. W., Zhang, J., Schweiger, A., Steele, M. A., & Stern, H. (2009). Arctic sea ice
731 retreat in 2007 follows thinning trend, Journal of Climate, 22, 165–176.
732 https://doi.org/10.1175/2008JCLI2521

733 Lindsay, R. W. (1998). Temporal variability of the energy balance of thick Arctic pack ice.
734 Journal of Climate, 11, 313–333.

735 Liu, Y., Key, J. R., Francis, J. A., & Wang, X. (2007). Possible causes of decreasing cloud
736 cover in the Arctic winter, 1982–2000, Geophysical Research Letter, 34, L14705.
737 https://doi.org/10.1029/2007GL030042

738 Liu, Y., Key, J. R., Liu, Z., Wang, X., & Vavrus, S. (2012). A cloudier Arctic expected with
739 diminishing sea ice. Geophysical Research Letter, 39, L05705.
740 https://doi.org/10.1029/2012GL051251

741 Liu, Y., & Key, J. R. (2014). Less winter cloud aids summer 2013 Arctic sea ice return from
742 2012 minimum. Environmental Research Letter, 9, 044002.
743 https://doi.org/10.1088/1748-9326/9/4/044002

744 Liu, Y., & Key, J. R. (2016). Assessment of arctic cloud cover anomalies in atmospheric
745 reanalysis products using satellite data, Journal of Climate, 29, 6065–6083.
746 https://doi.org/10.1175/JCLI-D-15-0861.1

747 Liu, Z., & Schweiger, A. (2017). Synoptic Conditions, Clouds, and Sea Ice Melt Onset in the
748 Beaufort and Chukchi Seasonal Ice Zone. Journal of Climate, 30, 6999–7016.

749 Markus, T., & Stroeve, J. C. (2009). Miller, J. Recent changes in Arctic sea ice melt onset,
750 freezeup, and melt season length. J. Geophys. Res., 114, C12.

751 Maslanik, J. A., Fowler, C., Stroeve, J., Drobot, S., Zwally, J., Yi, D., & Emery, W. (2007). A
752 younger, thinner Arctic ice cover: increased potential for rapid, extensive sea-ice loss.
753 Geophysical Research Letter, 34(24).

754 Maykut, G. A., & Untersteiner, N. (1971) Some results from a time-dependent thermodynamic
755 model of sea ice. Journal Geophysical Research, 76, 1550–1575.

756 Maykut, G. A. (1982). Large-scale heat exchange and ice production in the Central Arctic.
757 Journal Geophysical Research, 87, 7971–7984.

758 Minnis, P., Garber, D. P., Young, D. F., Arduini, R. F., & Takano, Y. (1998). Parameterization
759 of reflectance and effective emittance for satellite remote sensing of cloud
760 properties, Journal of Atmospheric Science, 55, 3313–3339.

761 Minnis, P., et al. (2011a). CERES Edition 2 cloud property retrievals using TRMM VIRS and
762 Terra and Aqua MODIS data: Part I: Algorithms. IEEE Transactions on Geoscience
763 and Remote Sensing Society, 49, 4374–4400.

764 Minnis, P., et al. (2011b), CERES Edition 2 cloud property retrievals using TRMM VIRS and
765 Terra and Aqua MODIS data: Part II: Examples of average results and comparisons
766 with other data. IEEE Transactions on Geoscience and Remote Sensing Society, 49,
767 4401–4430. https://doi.org/10.1108/TGRS.2011.2144601

768 Morrison, H., de Boer, G., Feingold, G., Harrington, J., Shupe, M. D., & Sulia, K. (2012).
769 Resilience of persistent Arctic mixed-phase clouds. Nature Geoscience, 5, 11–17.
770 https://doi.org/10.1038/ngeo1332

771 Morrison, A. L., Kay, J. E., Chepfer, H., Guzman, R., & Yettella, V. (2018). Isolating the
772 Liquid Cloud Response to Recent Arctic Sea Ice Variability Using Spaceborne Lidar
773 Observations. Journal of Geophysical Research, 123, 473–490.
774 https://doi.org/10.1002/2017JD027248

775 Mortin, J., Svensson, G., Graversen, R. G., Kapsch, M., Stroeve, J. C., & Boisvert, L. N. (2016).
776 Melt onset over Arctic sea ice controlled by atmospheric moisture transport.
777 Geophysical Research Letter, 43, 6636–6642.

778 Overland, J. E., & Wang, M. Y. (2010). Large-scale atmospheric circulation changes are
779 associated with the recent loss of Arctic sea ice. Tellus, Series A, 62, 1–9.
780 https://doi.org/10.1111/j.1600-0870.2009.00421.x

781 Palm, S. P., Strey, S. T., Spinhirne, J., & Markus, T. (2010). Influence of Arctic sea ice extent
782 on polar cloud fraction and vertical structure and implications for regional climate,
783 Journal of Geophysical Research, 115, D21209. https://doi.org/10.1029/2010JD013900

784 Parkinson, C. L. (2014). Spatially mapped reductions in the length of the Arctic sea ice season.
785 Geophysical Research Letter, 41, 4316–4322.

786 Pavelsky, T. M., Boé, J., Hall, A., & Fetzer, E. J. (2011). Atmospheric inversion strength over
787 polar oceans in winter regulated by sea ice. Climate Dynamics, 36, 945–955.
788 https://doi.org/10.1007/s00382-010-0756-8

789 Perovich, D. K., Nghiem, S. V., Markus, T., & Schweiger, A. (2007). Seasonal evolution and
790 interannual variability of the local solar energy absorbed by the Arctic sea ice-ocean
791 system. Journal of Geophysical Research, 112, C3.

792 Perovich, D. K., & Polashenski, C. (2012). Albedo evolution of seasonal Arctic sea ice,
793 Geophysical Research Letter, 39, L08501. https://doi.org/10.1029/2012GL051432

794 Persson, P. O. G., Fairall, C. W., Andreas, E. L., Guest, P. S., &. Perovich, D. K. (2002).
795 Measurements near the Atmospheric Surface Flux Group tower at SHEBA: Near-
796 surface conditions and surface energy budget. Journal of Geophysical Research:
797 Oceans, 107, 8045. https://doi.org/10.1029/2000JC000705

798 Persson, P. O. G. (2012). Onset and end of the summer melt season over sea ice: thermal
799 structure and surface energy perspective from SHEBA. Climate Dynamics, 39, 1349–
800 1371.

801 Persson, P. O. G., Shupe, M. D., Perovich, D., & Solomon, A. (2017). Linking atmospheric
802 synoptic transport, cloud phase, surface energy fluxes, and sea-ice growth: observations
803 of midwinter SHEBA conditions. Climate Dynamics, 49, 1341–1364.
804 https://doi.org/10.1007/s00382-016-3383-1

805 Rigor, I. G., Colony, R. L., & Martin, S. (2000). Variations in surface air temperature
806 observations in the Arctic, 1979–1997. Journal of Climate, 13, 896–914.

807 Sato, K., Inoue, J., Kodama, Y.-M., & Overland, J. E. (2012). Impact of Arctic sea-ice retreat
808 on the recent change in cloud-base height during autumn, Geophysical Research Letter,
809 39, L10503. https://doi.org/10.1029/2012GL051850

810 Slingo, J. M. (1987). The development and verification of a cloud prediction scheme for the
811 ECMWF model. Quarterly Journal of Royal Meteorological Society, 113, 899–927.

812 Schweiger, A. J., & Key, J. R. (1994). Arctic Ocean radiative fluxes and cloud forcing
813 estimated from the ISCCP C2 cloud dataset, 1983–1990. Journal of Applied
814 Meteorology, 33, 948–963. https://doi.org/10.1175/ 1520-
815 0450(1994)033,0948:AORFAC.2.0.CO;2

816 Schweiger, A. J., Lindsay, R. W., Vavrus, S., & Francis, J. A. (2008). Relationships between
817 Arctic sea ice and clouds during autumn, Journal of Climate, 21, 4799–4810.
818 https://doi.org/10.1175/2008JCLI2156.1

819 Screen, J. A., & Simmonds, I. (2010). The central role of diminishing sea ice in recent Arctic
820 temperature amplification. Nature, 464, 1334–1337.

821 Serreze, M. C., & Barry, R. G. (2011). Processes and impacts of Arctic amplification: A
822 research synthesis, Global and Planetary Change, 77, 85–96.

823 Serreze, M. C., Holland, M. M., & Stroeve, J. (2007). Perspectives on the Arctic's shrinking
824 sea-ice cover, Science, 315, 1533–1536. https://doi.org/10.1126/science.1139426

825 Shupe, M. D., & Intrieri, J. M. (2004). Cloud Radiative Forcing of the Arctic Surface: The
826 Influence of Cloud Properties, Surface Albedo, and Solar Zenith Angle. Journal of
827 Climate, 17, 616–628.

828 Shupe, M. D., Walden, V. P., Eloranta, E., Uttal, T., Campbell, J. R., Starkweather, S. M., &
829 Shiobara, M. (2011). Clouds at Arctic atmospheric observatories. Part I: Occurrence
830 and macrophysical properties. Journal of Applied Meteorogical Climatology, 50, 626–
831 644. https://doi.org/10.1175/2010JAMC2467.1

832 Smith, D. M. (1998). Observation of perennial Arctic sea ice melt and freeze-up using passive
833 microwave data, Journal of Geophysical Research, 103, 27753–27769.
834 https://doi.org/10.1029/98JC02416

835 Solomon, A., Shupe, M. D., Persson, M. D., & Morrison, H. (2011). Moisture and dynamical
836 interactions maintaining decoupled Arctic mixed phase stratocumulus in the presence
837 of a humidity inversion, Atmospheric Chemistry and Physics, 11, 10127–10148.
838 https://doi.org/10.5194/acp-11-10127-2011

839 Stroeve, J. C., Serreze, M. C., Holland, M. M., Kay, J. E., Malanik, J., & Barrett, A. P. (2012).
840 The Arctic's rapidly shrinking sea ice cover: A research synthesis. Climatic Change,
841 110, 1005–1027. https://doi.org/10.1007/s10584-011-0101-1

842 Stroeve, J. C., Markus, T., Boisvert, L., Miller, J., & Barrett, A. (2014). Changes in Arctic melt
843 season and implications for sea ice loss. Geophysical Research Letter, 41, 1216–1225.

844 Sun, Z., & Shine, K. P. (1994). Studies of the radiative properties of ice and mixed phase clouds,
845 Quarterly Journal of the Royal Meteorological Society, 120, 111–137.

846 Taylor, P. C., Kato, S., Xu, K.-M., & M. Cai (2015). Covariance between Arctic sea ice and
847 clouds within atmospheric state regimes at the satellite footprint level. Journal of
848 Geophysical Research: Atmosphere, 120, 12656–12678.

849 Taylor, P. C., Boeke, R. C., Li, Y., & Thompson, D. W. (2018). Arctic cloud annual cycle
850 biases in climate models. Atmospheric Chemistry and Physics. Discuss.
851 https://doi.org/10.5194/acp-2018-1159

852 Uppala, S., Dee, D., Kobayashi, S., Berrisford, P., & Simmons, A. (2008). Towards a climate
853 data assimilation system: status update of ERA-Interim. ECMWF Newsletter, 115, 12–
854 18.

855 Vavrus, S., Waliser, D., Schweiger, A., & Francis, J. (2009). Simulations of 20th and 21st
856 century Arctic cloud amount in the global climate models assessed in the IPCC AR4,
857 Climate Dynamics, 33, 1099–1115. https://doi.org/10.1007/s00382-008-0475-6

858 Vavrus, S., Holland, M. M., & Bailey, D. A. (2011). Changes in Arctic clouds during intervals
859 of rapid sea ice loss, Climate Dynamics, 36, 1475–1489.
860 https://doi.org/10.1007/s00382-010-0816-0

861 Vaughan, D. G., et al. (2013). Observations: cryosphere. In Stocker, TF and 9 others
862 eds Climate change 2013: the physical science basis. Contribution of Working Group I

863 to the Fifth Assessment Report of the Intergovernmental Panel on Climate
864 Change. Cambridge University Press, Cambridge and New York, 317–382.
865 https://doi.org/10.1017/CBO9781107415324.012

866 Vowinckel, E. (1962). Cloud amount and type over the Arctic. Arctic Meteorological Research
867 Group Publication 51. Montreal: McGill University. p. 27.

868 Wang, X., & Key, J. R. (2003). Recent trends in Arctic surface, cloud, and radiation properties
869 from space. Science, 299, 1725–1728.

870 Wang, X. J., & Key, J. R. (2005). Arctic surface, cloud, and radiation properties based on the
871 AVHRR Polar Pathfinder dataset. Part I: Spatial and temporal characteristics. Journal
872 of Climate, 18, 2558–2574. https://doi.org/10.1175/JCLI3438.1

873 Winton, M. (2006). Amplified Arctic climate change: What does surface albedo feedback have
874 to do with it? Geophysical Research Letter, 33, L03701.
875 https://doi.org/10.1029/2005GL025244

876 Wood, R., & Bretherton, C. S. (2006). On the relationship between stratiform low cloud cover
877 and lower-tropospheric stability. Journal of Climate, 19, 6425–6432.

878 Wood, R., & Hartmann, D. L. (2006). Spatial Variability of Liquid Water Path in Marine
879 Boundary Layer Clouds. Part I: the Importance of Mesoscale Cellular Convection.
880 Journal of Climate, 19, 1748–1764.

881 Wu, Q., & Zhang, X. (2010). Observed forcing-feedback processes between Northern
882 Hemisphere atmospheric circulation and Arctic sea ice coverage. Journal of
883 Geophysical Research, 115, D14119. https://doi.org/10.1029/2009JD013574

884 Wu, D. L., & Lee, J. N. (2012). Arctic low cloud changes as observed by MISR and CALIOP:
885 Implication for the enhanced autumnal warming and sea ice loss, Journal of
886 Geophysical Research, 117, D07107. https://doi.org/10.1029/2011JD017050

887 Wu, D. L., Zhang, J., Zhang, X., & Tao, W. (2014). Interannual variability and long-term
888 changes of atmospheric circulation over the Chukchi and Beaufort Seas. Journal of
889 Climate, 27, 4871–4889. https://doi.org/10.1175/JCLI-D-13-00610.1

890 Yoshimori, M., Abe-Ouchi, A., Watanabe, M., Oka, A., & Ogura, T. (2014). Robust
891 Seasonality of Arctic Warming Processes in Two Different Versions of the MIROC
892 GCM, Journal of Climate, 27, 6358–6375.

893 Zhang, T., Stamnes, K., & Bowling, S. A. (1996). Impact of clouds on surface radiative fluxes
894 and snowmelt in the Arctic and subarctic. Journal of Climate, 9, 2110–2123.

895 Zhang, X., Sorteberg, A., Jing, Z., Gerdes, R., & Comiso, J. C. (2008). Recent radical shifts of
896 atmospheric circulations and rapid changes in Arctic climate system. Geophysical
897 Research Letter, 35, L22701. https://doi.org/doi:10.1029/2008GL035607

898 Zhang, Y. Y., Stevens, B., Medeiros, B., & Ghil, M. (2009). Low-Cloud Fraction, Lower-
899 Tropospheric Stability, and Large-Scale Divergence. Journal of Climate, 22, 4827-4843.

Tables and Figure Captions:

Table 1. Annual means of the ice coverage (SIC), liquid and ice water content of the low-level cloud (LWP and IWP) and the total water content (TWP), cloud fraction (CF), water vapor below 3 km (WV), surface evaporation rate, lower tropospheric stability (LTS), and temperature at surface level (T_s) and 700hPa (T_{700hPa}) level over the four surface types and the sub-regions of *Transient Ice* region based on the melt season onset dates. For LWP, we also provide the annual mean averaged over regions that freeze after October, during October 16-31, October 1-15, and before October, in brackets placed from left to right.

Variable	**Surface type**							
	Permanent Ocean	*Transient Ice*					*Permanent Ice*	*Land*
		All	Melt before May 15	Melt in May 16-June 15	Melt in June 16-31	Melt after June		
SIC (%)	0.02	59.51	48.55	61.75	70.13	81.17	88.04	3.62
LWP (kg/m^2)	0.46	0.21	0.228 (0.236)	0.220 (0.227)	0.205 (0.212)	0.192 (0.189)	0.16	0.15
IWP (kg/m^2)	0.32	0.22	0.217	0.212	0.213	0.231	0.25	0.25
TWP (kg/m^2)	0.78	0.43	0.445	0.432	0.418	0.423	0.41	0.40
CF	0.348	0.263	0.268	0.263	0.257	0.264	0.246	0.194
WV (cm)	5.95	3.91	4.20	4.06	3.97	3.66	3.30	2.95
Evaporation rate (10^{-9} m/s)	7.656	0.992	1.509	1.205	0.910	0.663	0.608	0.742
LTS (K)	12.95	16.41	14.80	15.90	16.65	17.35	24.09	18.05
T_s (°C)	4.45	-10.35	-8.53	-9.63	-10.42	-11.61	-14.41	-17.68
T_{700hPa} (°C)	-13.47	-17.27	-16.54	-16.86	-17.13	-17.94	-18.49	-17.71

Figure captions:

Figure 1. Maps of (a) surface type. (b) and (c) are maps of sub-regions of the *Transient Ice* regions based on onset dates of (b) melt season and (c) freeze season.

Figure 2. Probability density function (PDF, units: %) of onset dates of melt season (red and pink bars) and onset dates of freeze season (blue and light blue bars) over all grid points in *Transient Ice* region. Red and blue bars indicate the PDF within the 10^{th} and the 90^{th} percentile.

Figure 3. Map of climatological annual mean of sea ice concentration (SIC, units: %).

Figure 4. Seasonal cycle of PDF (units: %) of SIC over different regions grouped based on the onset of melt season (a–d), and those grouped based on the onset date of freeze date (e–h), and over all grid points (i). Black curve indicates the mean value.

Figure 5. Annual cycle of PDF (shadings) and mean value (black curve) of total cloud LWP in lower layers below 3 km (units: kg/m^2) over four surface types as indicated by Fig. 1a: (a) *Permanent Ocean*, (b) *Transient Ice*, (c) *Permanent Ice*, (d) *land*, as well as over four sub-regions of *Transient Ice* with different (e-h) melt and (i-l) freeze season onset dates as indicated by Fig. 1b. Contours indicate the difference of the PDF for each sub-type with the PDF over all grid points belonging to *Transient Ice* type as shown in Fig. 5b. Positive difference is presented by the red solid contours while negative difference is presented by the blue dashed contours. Contour levels are $\pm 2,\ \pm 5,\ \pm 8$.

Figure 6. The same as Fig. 5, but for the water vapor in lower layers below 3km.

Figure 7. The same as Fig. 5, but for the surface evaporation rate (units: 10^9 m/s) derived from ERA Interim Reanalysis.

Figure 8. The same as Fig. 5, but for the lower tropospheric static stability (LTS, units: K).

Figure 9. Annual cycle of PDF (shadings) and mean value (black curve) of surface temperature (units: °C) over four surface types as indicated by Fig. 1a: (a) *Permanent Ocean*, (b) *Transient Ice*, (c) *Permanent Ice*, (d) *land*, as well as over (e-h) four sub-regions of *Transient Ice* with different melt season onset dates as indicated by Fig. 1b. Contours in left panels indicate the difference of the PDF for each type with the PDF over *Land* surface as shown in Fig. 8d, with contour levels at $\pm 5,\ \pm 10,\ \pm 20$. Grey curves overlaid in panels a–c is the mean seasonal variation of surface temperature over *Land* surface. Contours in the right panels indicate the difference of the PDF for each sub-region with the PDF over all grid points belonging to *Transient Ice* type as shown in Fig. 8b, with contour levels at $\pm 2,\ \pm 5,\ \pm 8$.

Figure 10. The same as Fig. 9, but for the temperature at 700 hPa (units: °C).

Figure 11. Correlations of low-level cloud LWP with (a) total water vapor below 3km, and (b) LTS during the months in the melt season, i.e., April to October.

Figure 12. The same as Fig. 5, but for the cloud ice water path (IWP) in lower layers below 3 km (units: kg/m^2).

946

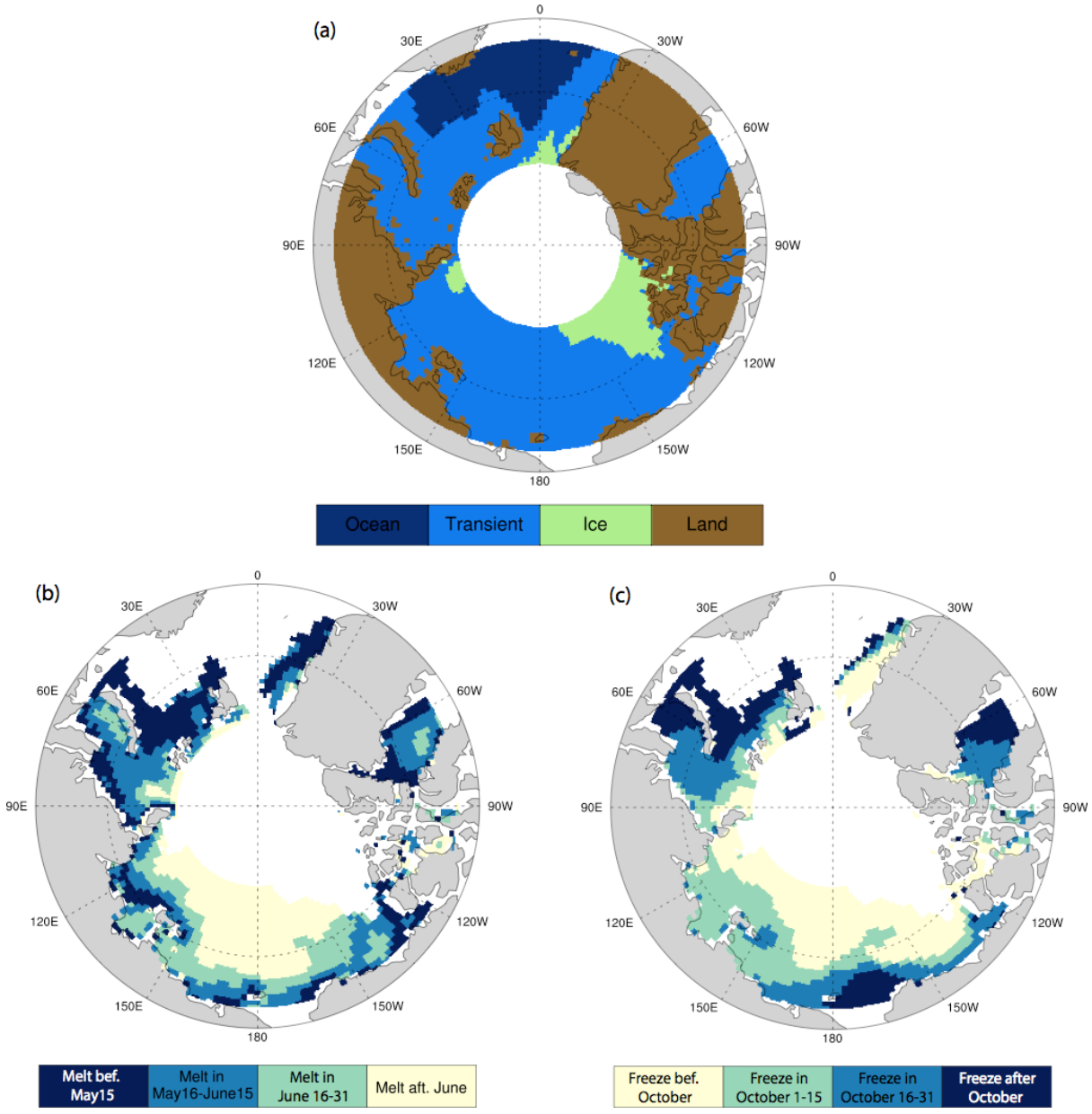

947

948 **Figure 1.** Maps of (a) surface type. (b) and (c) are maps of sub-regions of the *Transient Ice*
949 regions based on onset dates of (b) melt season and (c) freeze season.

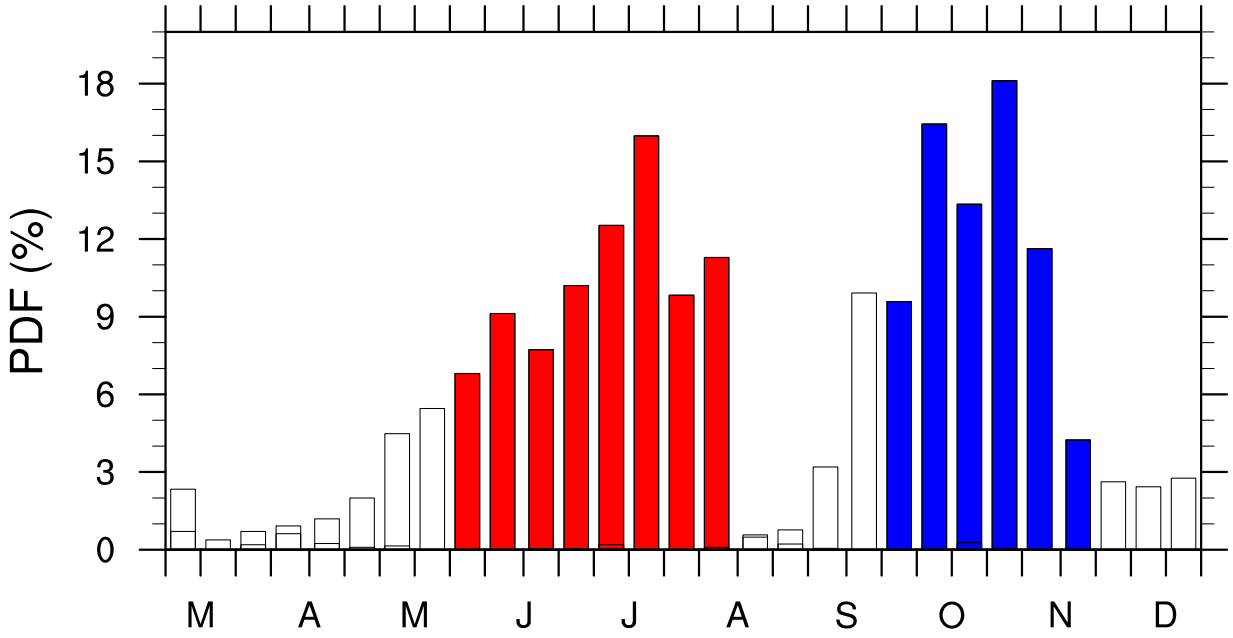

Figure 2. Probability density function (PDF, units: %) of onset dates of melt season (red and pink bars) and onset dates of freeze season (blue and light blue bars) over all grid points in *Transient Ice* region. Red and blue bars indicate the PDF within the 10^{th} and the 90^{th} percentile.

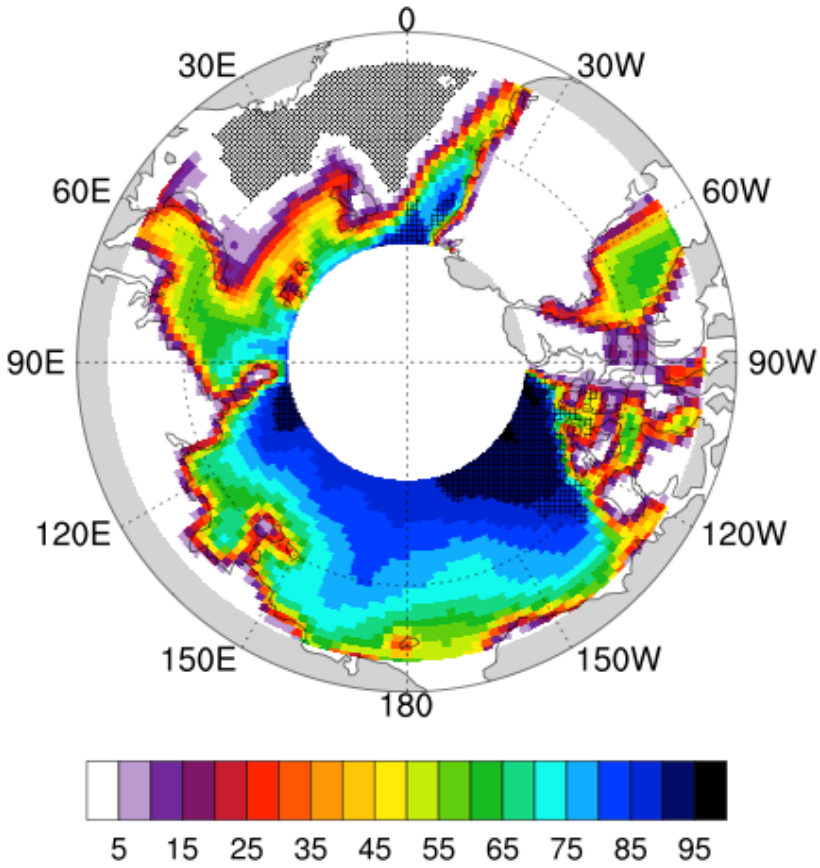

954

955 **Figure 3.** Map of climatological annual mean of sea ice concentration (SIC, units: %).

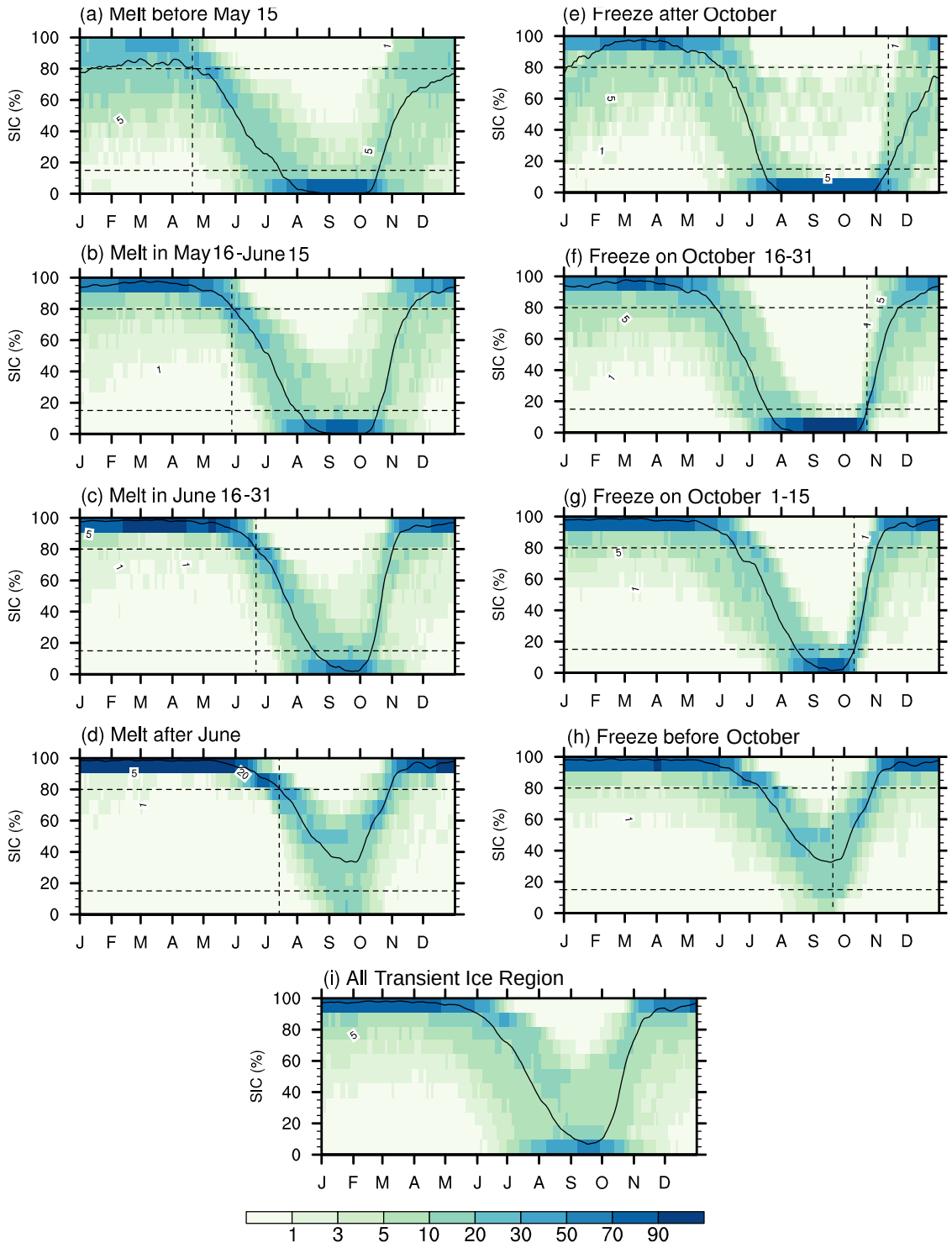

Figure 4. Seasonal cycle of probability density function (PDF, units: %) of SIC over different regions grouped based on the onset of melt season (a–d), and those grouped based on the onset date of freeze date (e–h), and over all grid points (i). Black curve indicates the mean value.

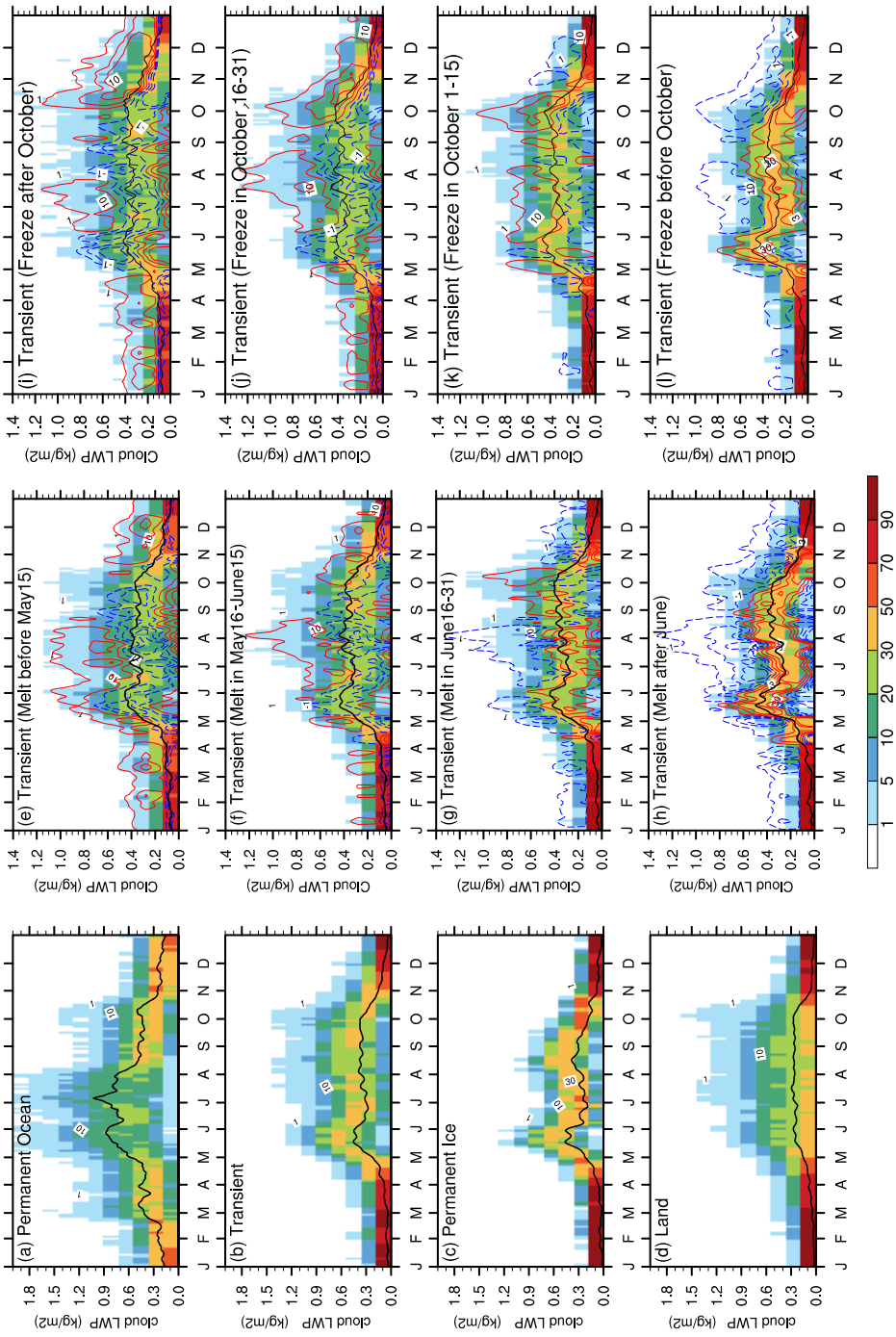

Figure 5. Annual cycle of PDF (shadings) and mean value (black curve) of total cloud LWP in lower layers below 3 km (units: kg/m^2) over four surface types as indicated by Fig. 1a: (a) *Permanent Ocean*, (b) *Transient Ice*, (c) *Permanent Ice*, (d) *land*, as well as over four sub-regions of *Transient Ice* with different (e-h) melt and (i-l) freeze season onset dates as indicated by Fig. 1b. Contours indicate the difference of the PDF for each sub-type with the PDF over all grid points belonging to *Transient Ice* type as shown in Fig. 5b. Positive difference is presented by the red solid contours while negative difference is presented by the blue dashed contours. Contour levels are ± 2, ± 5, ± 8.

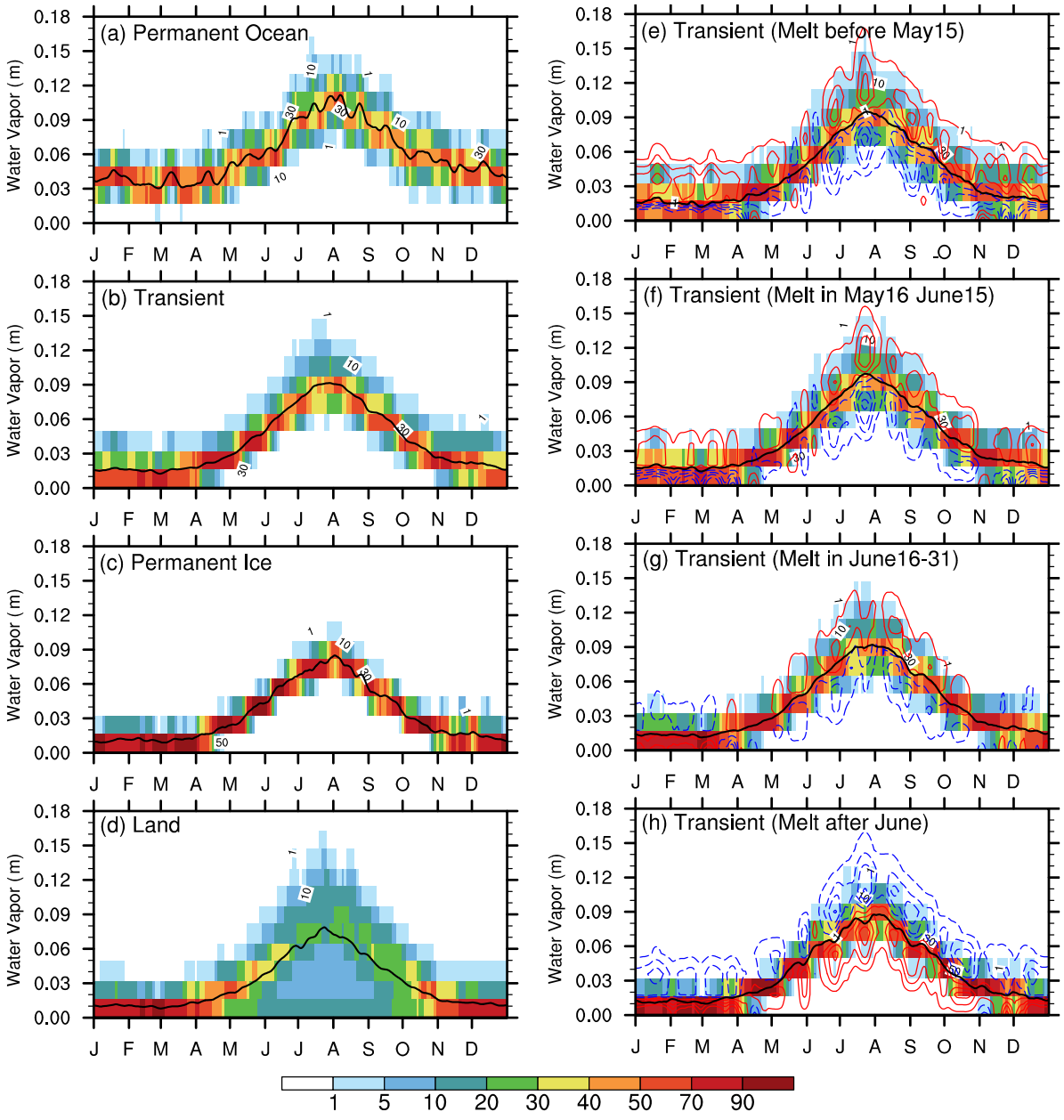

Figure 6. The same as Fig. 5, but for the water vapor in lower layers below 3km.

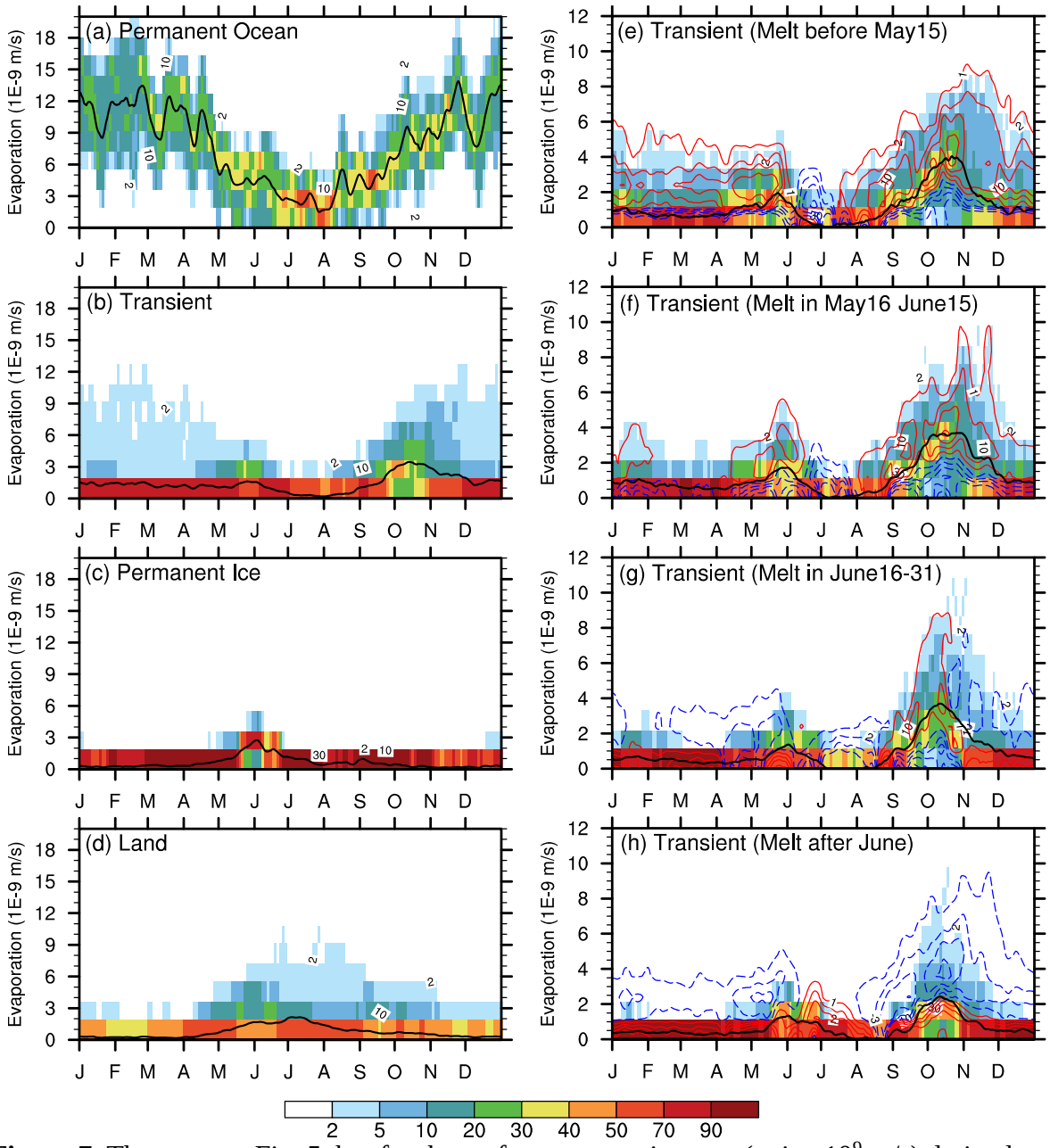

977
978 **Figure 7.** The same as Fig. 5, but for the surface evaporation rate (units: 10^9 m/s) derived
979 from ERA Interim Reanalysis.

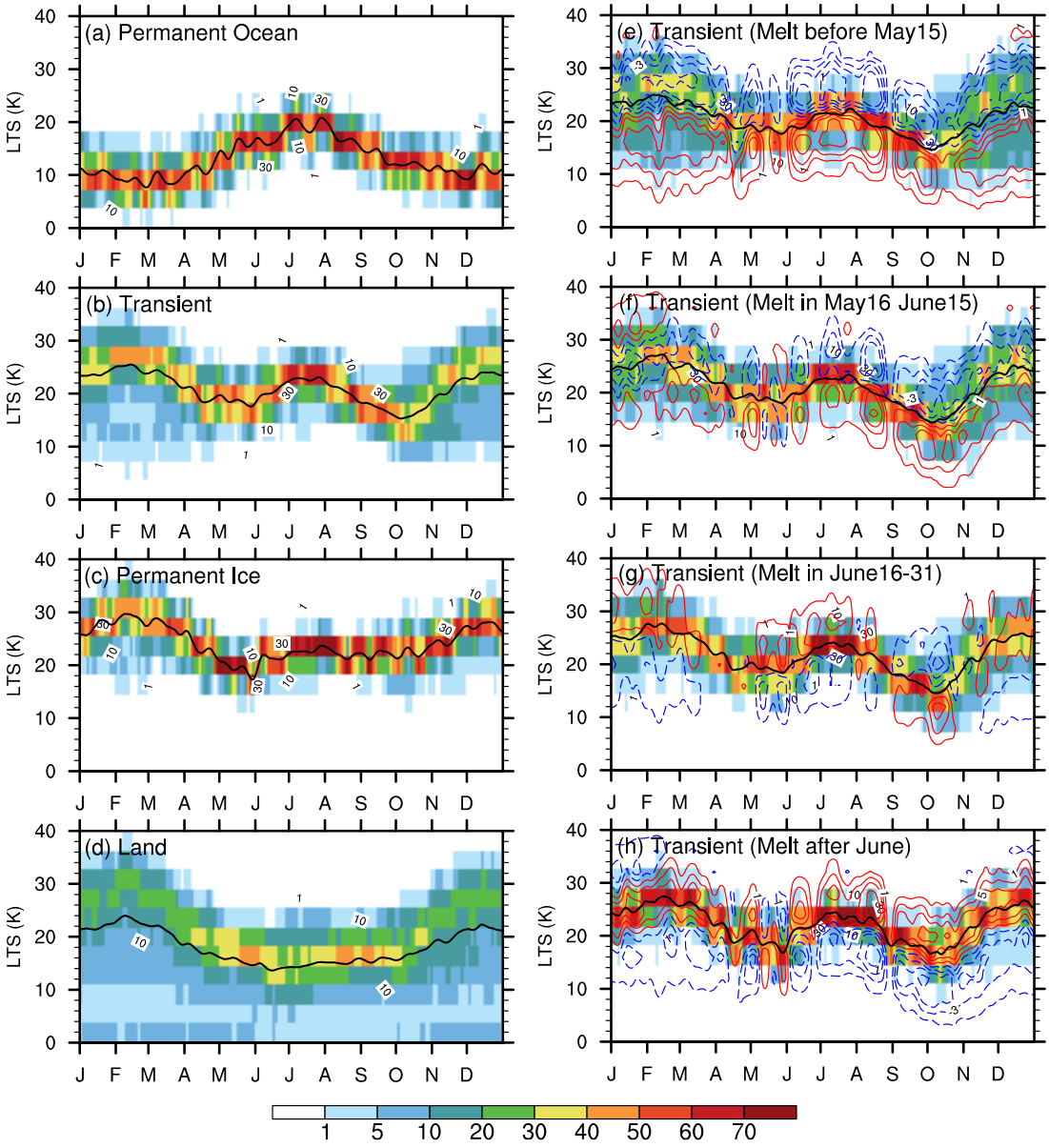

Figure 8. The same as Fig. 5, but for the lower tropospheric static stability (LTS, units: K).

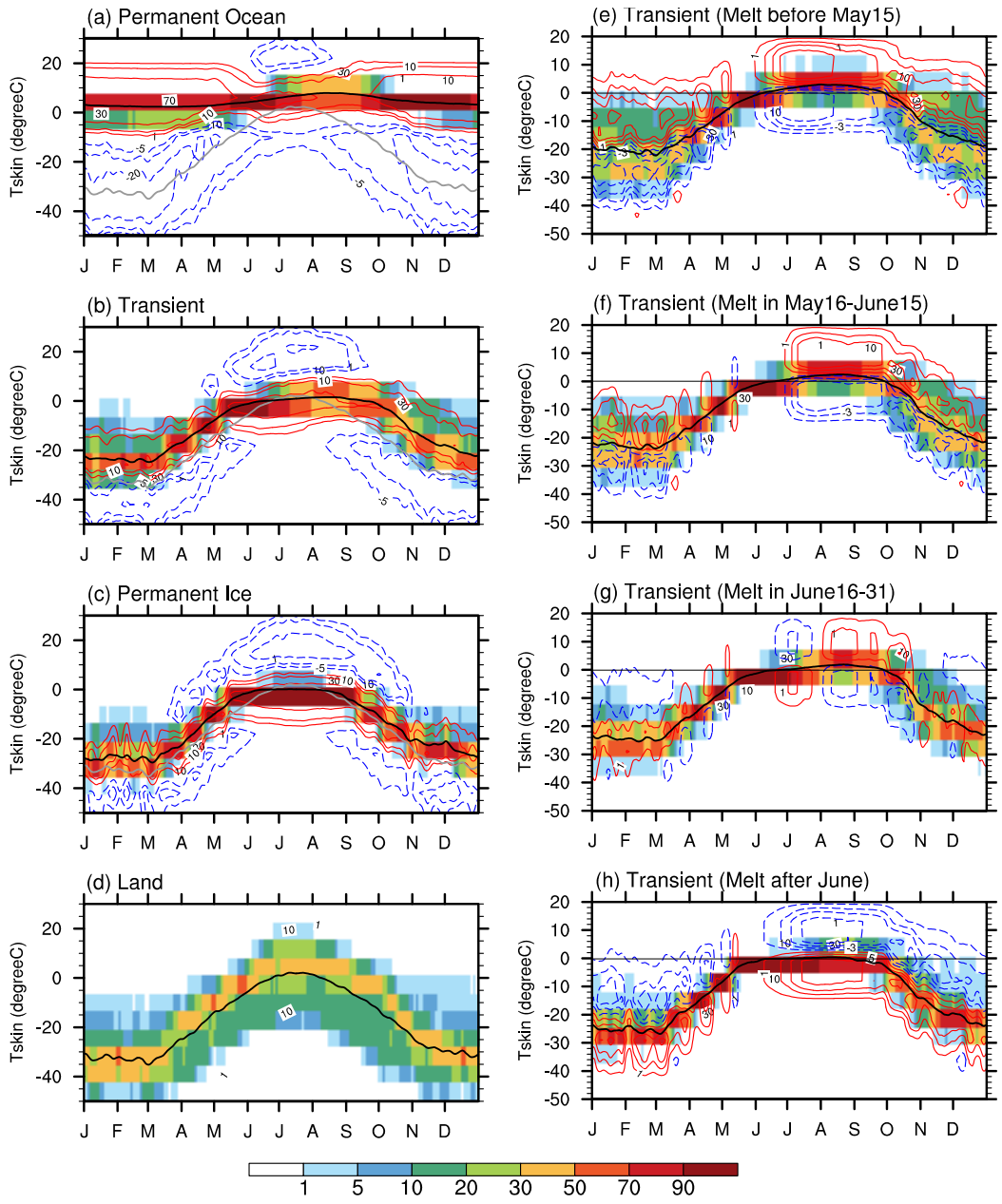

Figure 9. Annual cycle of PDF (shadings) and mean value (black curve) of surface temperature (units: °C) over four surface types as indicated by Fig. 1a: (a) *Permanent Ocean*, (b) *Transient Ice*, (c) *Permanent Ice*, (d) *land*, as well as over (e-h) four sub-regions of *Transient Ice* with different melt season onset dates as indicated by Fig. 1b. Contours in left panels indicate the difference of the PDF for each type with the PDF over *Land* surface as shown in Fig. 8d, with contour levels at ± 5, ± 10, ± 20. Grey curves overlaid in panels a–c is the mean seasonal variation of surface temperature over *Land* surface. Contours in the right panels indicate the difference of the PDF for each sub-region with the PDF over all grid points belonging to *Transient Ice* type as shown in Fig. 8b, with contour levels at ± 2, ± 5, ± 8.

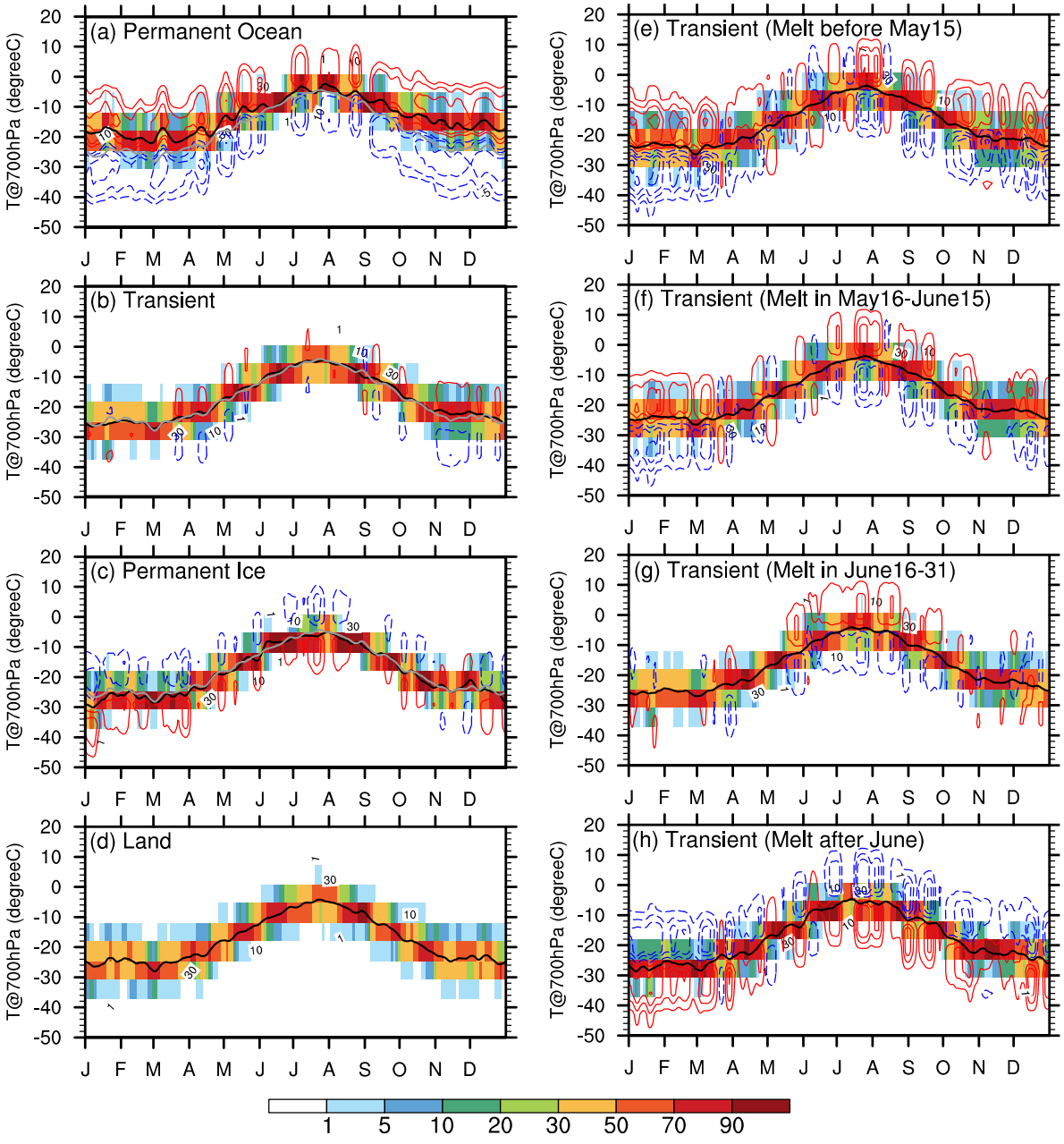

995

996

997 **Figure 10.** The same as Fig. 9, but for the temperature at 700 hPa (units: °C).

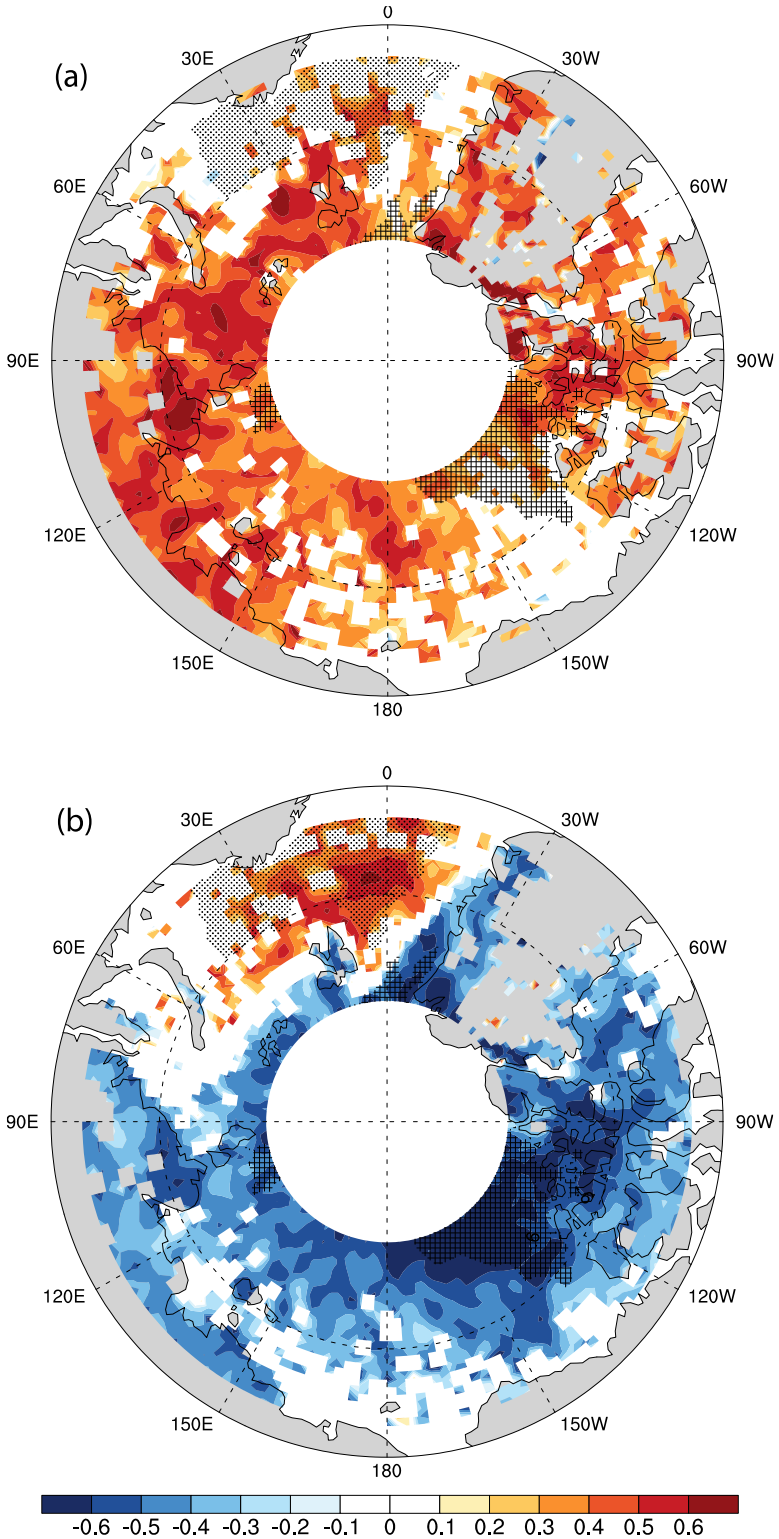

998
999

1000 **Figure 11.** Correlations of low-level cloud LWP with (a) total water vapor below 3km, and
1001 (b) LTS during the months in the melt season, i.e., April to October.

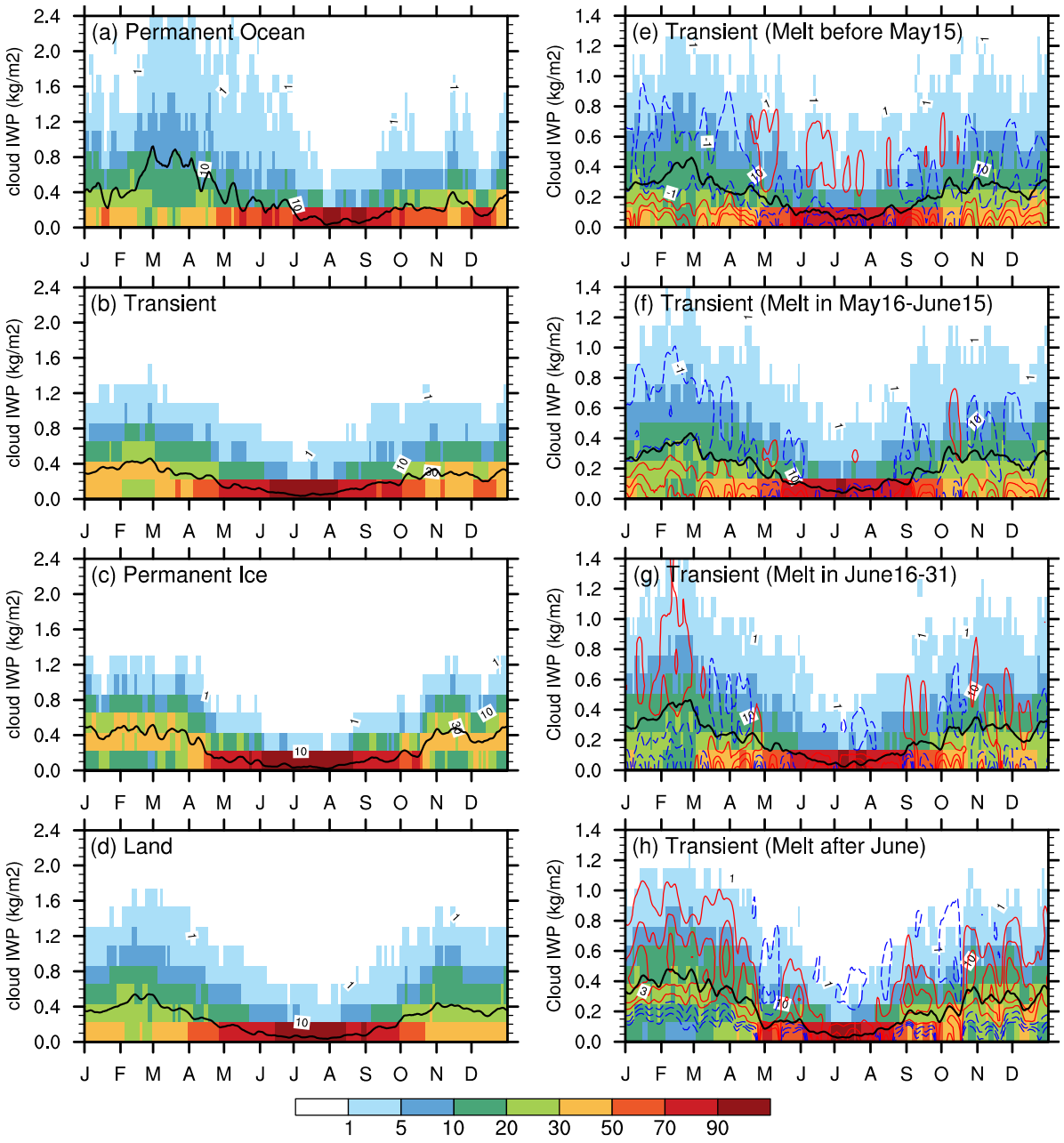

Figure 12. The same as Fig. 5, but for the cloud ice water path (IWP) in lower layers below 3 km (units: kg/m^2).